Keep it Together: Modelling Myeloma Dissemination *in vitro* with hMSC-Interacting Subpopulations of INA-6 Cells and their Aggregation/Detachment Dynamics

Martin Kuric[1], Susanne Beck[2], Doris Schneider[1], Wyonna Rindt[3], Marietheres Evers[4], Jutta Meißner-Weigl[1], Sabine Zeck[1], Melanie Krug[1], Marietta Herrmann[5], Tanja Nicole Hartmann[6], Ellen Leich[4], Maximilian Rudert[7], Denitsa Docheva[1], Anja Seckinger[8], Dirk Hose[8], Franziska Jundt[3], Regina Ebert[1]

[1]University of Würzburg, Department of Musculoskeletal Tissue Regeneration, Würzburg, Germany

[2]University Hospital Heidelberg, Institute of Pathology, Heidelberg, Germany

[3]University Hospital Würzburg, Department of Internal Medicine II, Würzburg, Germany

[4]University of Würzburg, Institute of Pathology, Comprehensive Cancer Center Mainfranken, Würzburg, Germany

[5]University Hospital Würzburg, IZKF Research Group Tissue Regeneration in Musculoskeletal Diseases, Würzburg, Germany

[6]University of Freiburg, Department of Internal Medicine I, Faculty of Medicine and Medical Center, Freiburg, Germany

[7]University of Würzburg, Orthopedic Department, Clinic König-Ludwig-Haus, Würzburg, Germany

[8]Vrije Universiteit Brussel, Department of Hematology and Immunology, Jette, Belgium

Running Title

Keep it Together: Modelling Myeloma Dissemination *in vitro*

Keywords

Multiple Myeloma, Human Mesenchymal Stromal Cells (hMSC), Cell Adhesion, Dissemination, Survival

Additional Information

Corresponding Authors:

Martin Kuric, Department of Musculoskeletal Tissue Regeneration, Julius-Maximilians-Universität Würzburg, Friedrich-Bergius-Ring 15, 97076 Würzburg, Germany, Phone +49 931 803 1583, martin.kur4@gmail.com

Prof. Dr. Regina Ebert, Department of Musculoskeletal Tissue Regeneration, Julius-Maximilians-Universität Würzburg, Friedrich-Bergius-Ring 15, 97076 Würzburg, Germany, Phone +49 931 803 1597, regina.ebert@uni-wuerzburg.de

Conflict of Interest:

The authors declare no potential conflicts of interest.

Abstract

Multiple myeloma involves early dissemination of malignant plasma cells across the bone marrow; however, the initial steps of dissemination remain unclear. Human bone marrow-derived mesenchymal stromal cells (hMSCs) stimulate myeloma cell expansion (e.g., IL-6) and simultaneously retain myeloma cells via chemokines (e.g., CXCL12) and adhesion factors. Hence, we hypothesized that the imbalance between cell division and retention drives dissemination.

We present an *in vitro* model using primary hMSCs co-cultured with INA-6 myeloma cells. Time-lapse microscopy revealed proliferation and attachment/detachment dynamics. Separation techniques (V-well adhesion assay and well plate sandwich centrifugation) were established to isolate MSC-interacting myeloma subpopulations that were characterized by RNAseq, cell viability and apoptosis. Results were correlated with gene expression data (n=837) and survival of myeloma patients (n=536).

On dispersed hMSCs, INA-6 saturate hMSC-surface before proliferating into large homotypic aggregates, from which single cells detached completely. On confluent hMSCs, aggregates were replaced by strong heterotypic hMSC-INA-6 interactions, which modulated apoptosis time-dependently. Only INA-6 daughter cells (nMA-INA6) detached from hMSCs by cell division but sustained adherence to hMSC-adhering mother cells (MA-INA6).

Isolated nMA-INA6 indicated hMSC-autonomy through superior viability after IL-6 withdrawal and upregulation of proliferation-related genes. MA-INA6 upregulated adhesion and retention factors (*CXCL12*), that, intriguingly, were highly expressed in myeloma samples from patients with longer overall and progression-free survival, but their expression decreased in relapsed myeloma samples.

Altogether, *in vitro* dissemination of INA-6 is driven by detaching daughter cells after a cycle of hMSC-(re)attachment and proliferation, involving adhesion factors that represent a bone marrow-retentive phenotype with potential clinical relevance.

Statement of Significance

Novel methods describe *in vitro* dissemination of myeloma cells as detachment of daughter cells after cell division. Myeloma adhesion genes were identified that counteract *in vitro* detachment with potential clinical relevance.

Introduction

Multiple myeloma arises from clonal expansion of malignant plasma cells in the bone marrow (BM). At diagnosis, myeloma cells have disseminated to multiple sites in the skeleton and, in some cases, to “virtually any tissue” (1, 2). However, the mechanism through which myeloma cells initially disseminate remains unclear.

Dissemination is a multistep process involving invasion, intravasation, intravascular arrest, extravasation, and colonization (3). To initiate dissemination, myeloma cells overcome adhesion, retention, and dependency on the BM microenvironment, which could involve the loss of adhesion factors such as CD138 (4, 5). BM retention is mediated by multiple factors: First, chemokines (CXCL12 and CXCL8) produced by mesenchymal stromal cells (MSCs), which attract plasma cells and prime their cytoskeleton and integrins for adhesion (6, 7). Second, myeloma cells must overcome the anchorage and physical boundaries of the extracellular matrix (ECM), consisting of e.g. fibronectin, collagens, and proteoglycans such as decorin (8-11). Simultaneously, ECM provides signals inducing myeloma cell cycle arrest or progression the cell cycle (8, 10). ECM is also prone to degradation, which is common in several osteotropic cancers, and is the cause of osteolytic bone disease. This is driven by a ‘vicious cycle’ that maximizes bone destruction by extracting growth factors (EGF and TGF-β) that are stored in calcified tissues (12). Third, direct contact with MSCs physically anchors myeloma cells to the BM (3, 13). Fourth, to disseminate to distant sites, myeloma cells require, at least partially, independence from essential growth and survival signals provided by MSCs in the form of soluble factors or cell adhesion signaling (5, 14, 15). For example, the VLA4 (Myeloma)–VCAM1 (MSC)-interface activates NF-κB in both myeloma and MSCs, inducing IL-6 expression in MSCs. The independence from MSCs is then acquired through autocrine survival signaling (16, 17). In short, anchorage of myeloma cells to MSCs or ECM is a ‘double-edged sword’: adhesion counteracts dissemination, but also presents signaling cues for growth, survival, and drug resistance (18).

To address this ambiguity, we developed an *in vitro* co-culture system modeling diverse adhesion modalities to study dissemination, growth, and survival of myeloma cells and

hMSCs. Co-cultures of hMSCs and the myeloma cell line INA-6 replicated tight interactions and aggregate growth, akin to "microtumors" in Ghobrial's metastasis concept (19). We characterized the growth conformations of hMSCs and INA-6 as homotypic aggregation *vs.* heterotypic hMSC adherence and their effects on myeloma cell survival. We tracked INA-6 detachments from aggregates and hMSCs, thereby identifying a potential "disseminated" subpopulation lacking strong adhesion. We developed innovative techniques (V-well adhesion assay and well plate sandwich centrifugation) to separate weakly and strongly adherent subpopulations for the subsequent analysis of differential gene expression and cell survival. Notably, our strategy resolves the differences in gene expression and growth behavior between cells of one cell population in "direct" contact with MSCs. In contrast, previous methods differentiated between "direct" and "indirect" cell-cell contact using transwell inserts (20). To evaluate whether genes mediating adhesion and growth characteristics of INA-6 were associated with patient survival, we analyzed publicly available datasets (21, 22).

Materials and Methods

See supplemental for a complete method list and description.

Ethics Statement

Primary human MSCs were collected with informed consent from all patients and the procedure was approved by the local Ethics Committee of the University of Würzburg (186/18).

Cultivation and Co-Culturing of primary hMSCs and INA-6

Cell isolation, cultivation, and medium composition are provided in the supplemental materials and methods section. Primary human MSCs (hMSC) were obtained from 34 non-myeloma patients undergoing elective hip arthroplasty (Tab. S1:21 male and 13 female, mean age 68.9 ± 10.6). The INA-6 cell line (DSMZ Cat# ACC-862, RRID:CVCL_5209, link) was initially isolated from a pleural effusion sample obtained from an 80-year-old male with multiple myeloma (23, 24). hMSCs were not tested for mycoplasma, whereas stocks of INA-6

were tested in this study (Tab. S1) using the Venor GeM OneStep kit (Minerva Biolabs, Berlin, Germany).

For each co-culture, hMSCs were seeded 24 h before INA-6 addition to generate the MSC-conditioned medium (CM). INA-6 cells were washed with PBS, resuspended in MSC medium, and added to hMSCs so that the co-culture comprised 33% (v/v) of CM gathered directly from the respective hMSC donor. The co-cultures were not substituted for IL-6 (14).

Cell Viability and Apoptosis Assay

Cell viability and apoptosis rates were measured using CellTiter-Glo Luminescent Cell Viability Assay and Caspase-Glo 3/7 Assay, respectively (Promega GmbH, Mannheim, Germany).

Automated Fluorescence Microscopy

Microscopic images were acquired using an Axio Observer 7 (Zeiss) with a COLIBRI LED light source and motorized stage top using 5x and 10x magnification. The tiled images had an automatic 8-10% overlap and were not stitched.

Live Cell Imaging

hMSCs (stained with PKH26) were placed into an ibidi Stage Top Incubation System and equilibrated to 80% humidity and 5% CO_2. INA-6 (2×10^3 cells/cm^2) were added directly before the start of acquisition. Brightfield and fluorescence images of up to 13 mm^2 of the co-culture area were acquired every 15 min for 63 h. Each event of interest was manually analyzed and categorized into defined event parameters.

V-well Adhesion Assay

INA-6 cells were arrested during mitosis by two treatments with thymidine, followed by nocodazole. Arrested INA-6 were released and added to 96 V-well plates (10^4 cells/cm^2) on top of confluent hMSCs and adhered for 1-3 h. The co-culture was stained with calcein-AM (Thermo Fisher Scientific, Darmstadt, Germany) before non-adherent INA-6 were pelleted into the tip of the V-well (2000 rpm, 5-10 min). MSC-adhering INA-6 cells were manually detached by rapid pipetting. The pellet brightness was measured microscopically and the pellet was isolated by pipetting.

Cell Cycle Profiling by Image Cytometry

Isolated INA-6 cells were fixed in 70% ice-cold ethanol, washed, resuspended in PBS, distributed in 96-well plates, and stained with Hoechst-33342. The plates were scanned at 5x magnification. A pre-trained convolutional neural network (Intellesis, Zeiss) was fine-tuned to segment the scans into single nuclei and exclude fragmented nuclei. Nuclei were filtered to exclude extremes of size roundness. The G0/G1 frequency was determined by Gaussian curve fitting.

Well Plate Sandwich Centrifugation (WPSC)

hMSCs were grown to confluence in 96-well plates coated with collagen I (rat tail; Corning, NY, USA). INA-6 were added and the cells were allowed to adhere for 24 h. A second plate ("catching plate") was attached upside down to the top of the co-culture plate. That "well plate sandwich" was turned around and the content of the co-culture plate was centrifuged into the catching plate three times (40 seconds at 110 g) while gently adding 30 µL of medium in between centrifugation steps. Non-MSC-adhering INA-6 cells were collected from the catching plate, whereas MSC-adhering INA-6 cells were isolated by digesting the co-culture with Accutase. For RNA sequencing (RNAseq), all samples were purified using anti-CD45 magnetic-assisted cell sorting (Miltenyi Biotec B.V. & Co. KG, Bergisch Gladbach).

RNA Isolation

RNA was isolated using the NucleoSpin RNA II Purification Kit (Macherey-Nagel) according to the manufacturer's instructions. RNA was isolated from INA-6 cells co-cultured with a unique hMSC donor (n=5 for qPCR n=11).

RNA sequencing, Differential Expression, and Functional Enrichment Analysis

RNAseq was performed at the Core Unit Systems Medicine, University of Würzburg. mRNA was enriched with polyA beads. Fastq files were aligned to the GRCh38 reference genome using STAR (RRID:SCR_004463, link) and raw read counts were generated using HTseq (25-27). Differential gene expression was analyzed using edgeR in R (version 3.6.3). Functional enrichment analysis was performed using Metascape (28).

RT-qPCR

RNA (1 µg) was reverse transcribed using SuperScript IV reverse transcriptase (Thermo Fisher Scientific, Darmstadt, Germany). qPCR was performed using 10 µL GoTaq qPCR Master Mix (Promega), 1:10 diluted cDNA, and 5 pmol of primers obtained from Biomers.net or Qiagen (Tab. S3).

Statistics

Inferential statistics were performed using Python (IPython, RRID:SCR_001658, link) (3.10) packages pingouin (0.5.1) and statsmodels (0.14.0) (29, 30). The figures were plotted using plotastic (0.0.1) (31). Normality (for $n \geq 4$) and sphericity were ensured using Mauchly's and Shapiro-Wilk tests, respectively. Data points were log10 transformed to convert the scale from multiplicative to additive or to fulfill sphericity requirements. p-value = 0.05 > * > 0.01 > ** > 10^{-3} > *** 10^{-4} > ****. P-values were either adjusted (p-adj) or not adjusted (p-unc) for family wise error rate. Power calculations were not performed to determine the sample size.

Patient Cohort, Analysis of Survival and Expression

Survival and gene expression data were obtained as previously described (21, 22) and are available at the European Nucleotide Archive (ENA) under accession numbers PRJEB36223 and PRJEB37100. The expression level was categorized into "high" and "low" using maxstat (Maximally selected Rank Statistics) thresholds (32).

Data Availability Statement

A detailed description of the methods is provided in the Supplementary Material section. Raw tabular data and examples of analyses and videos are available in the github repository (33). Raw RNAseq data are available from the NCBI Gene Expression Omnibus (GEO) (RRID:SCR_005012, link) (GSExxxxx). Microscopy data are available at the Image Data Resource (IDR) (RRID:SCR_017421, link) (idrxxxx).

Results

INA-6 Cells Saturate hMSC-Interaction to Proliferate into Aggregates

hMSCs are isolated as a heterogeneous cell population. To analyze whether INA-6 cells could adhere to every hMSC, we saturated hMSCs with INA-6. A seeding ratio of 1:4

(hMSC:INA-6) resulted in the occupation of 93% ± 6% of single hMSCs by one or more INA-6 cells within 24 h after INA-6 addition, escalating to 98% after 48 h (Fig. 1A, B). Therefore, most hMSCs provide an interacting surface for INA-6 cells.

INA-6 exhibits homotypic aggregation when cultured alone, a phenomenon observed in some freshly isolated myeloma samples (up to 100 cells after 6 h) (34, 35). Adding hMSCs at a 1:1 ratio led to smaller aggregates after 24 h (size 1-5 cells), all of which were distributed over 52 ± 2% of all hMSCs (Fig. 1A, B). Intriguingly, INA-6 aggregation was notably absent when grown on confluent hMSCs, and occurred only when heterotypic interactions were limited to 0.2 hMSCs per INA-6 cell (Fig. 1C). We concluded that INA-6 cells prioritize heterotypic over homotypic interactions.

To monitor the formation of such aggregates, we conducted live-cell imaging of hMSC/INA-6 co-cultures for 63 h. We observed that INA-6 cells adhered long after cytokinesis, constituting 55 ± 12% of all homotypic interactions between 13 and 26 h, increasing to >75% for the remainder of the co-culture (Fig. 1D). Therefore, homotypic INA-6 aggregates were mostly formed by cell division.

Apoptosis of INA-6 Depends on Ratio Between Heterotypic and Homotypic Interaction

Although direct interaction with hMSCs has been shown to enhance myeloma cell survival through NF-κB signaling (15), the impact of aggregation on myeloma cell viability during hMSC interaction remains unclear. To address this, we measured the cell viability (ATP) and apoptosis rates of INA-6 cells growing as homotypic aggregates compared to those in heterotypic interactions with hMSCs by modulating hMSC density (Fig. 1E). To equalize the background signaling caused by soluble MSC-derived factors, all cultures were incubated in hMSC-conditioned medium and the results were normalized to INA-6 cells cultured without direct hMSC contact (Fig. 1E, left).

INA-6 viability (ATP) was not affected by the direct adhesion of hMSCs at any density. However, apoptosis rates decreased over time [$F(2, 6) = 23.29$, p-unc = 1.49e-03, Two-factor RM-ANOVA], interacting significantly with MSC density [$F(4, 12) = 6.98$, p-unc = 3.83e-3]. For example, 24 h of adhesion to confluent MSCs increased apoptosis rates by 1.46 ± 0.37

fold, while culturing INA-6 cells on dispersed hMSCs (ratio 1:1) did not change the apoptosis rate (1.01 ± 0.26).

We presumed that sensitive apoptotic cells might have been lost when harvesting INA-6 cells from hMSCs. Hence, we measured survival parameters in the co-culture and in hMSC and INA-6 cells cultured separately (Fig. 1E, right). We defined MSC interaction effects when the survival measured in the co-culture differed from the sum of the signals measured from INA-6 and hMSCs alone. RM-ANOVA confirmed that adherence to confluent MSCs increased apoptosis rates of INA-6 cells 24 h after adhesion and decreased after 72 h [interaction between MSC density and time: $F(2, 4) = 26.86$, p-unc = 4.80e-03, Two-factor RM-ANOVA], whereas INA-6 cells were unaffected when grown on dispersed hMSCs.

In summary, the growth conformation of INA-6 cells, measured as the ratio between homotypic aggregation and heterotypic MSC interactions, affected apoptosis rates of INA-6 cells.

Single INA-6 Cells Detach Spontaneously from Aggregates of Critical Size

Using time-lapse microscopy, we observed that 26 ± 8% of INA-6 aggregates growing on single hMSCs spontaneously shed INA-6 cells (Fig. 2A, B; Vid. S1). Notably, all detached cells exhibited similar directional movements, suggesting entrainment in convective streams generated by temperature gradients within the incubation chamber. INA-6 predominantly detached from other INA-6 cells or aggregates (Fig. 2C), indicating weaker adhesive forces in homotypic interactions than in heterotypic interactions. The detachment frequency increased after 52 h, when most aggregates that shed INA-6 cells were categorized as large (> 30 cells) (Fig. 2D). Since ~1020 INA6 cells already fully covered a single hMSC, we suggest that myeloma cell detachment depended not only on hMSC saturation, but also required a minimum aggregate size. Interestingly, INA-6 detached mostly as single cells, independent of aggregate size categories [$F(2, 6)=4.68$, p- unc=.059, Two-factor RM-ANOVA] (Fig. 2D), showing that aggregates remained mostly stable despite losing cells.

Cell Division Generates a Daughter Cell Detached from hMSC

We suspected that cell division drives detachment because we observed that MSC-adhering INA-6 cells could generate daughter cells that “roll over” the mother cell (Fig. 3A; Vid. S2). We recorded and categorized the movement of INA-6 daughter cells in confluent hMSCs after cell division. Half of all INA-6 divisions yielded two daughter cells that remained stationary, indicating hMSC adherence (Fig. 3B, C; Vid. S3). The other half of division events generated one hMSC-adhering (MA) cell and one non-hMSC-adhering (nMA) cell, which rolled around the MA cell for a median time of 2.5 h post division (Q_1=1.00 h, Q_3=6.25 h) until it stopped and re-adhered to the hMSC monolayer (Fig. 3D; Vid. S2, S4). Thus, cell division establishes a time window in which one daughter cell can detach.

To validate that cell division reduced adhesion, we measured both the size and cell cycle profile of the nMA and MA populations using an enhanced V-well assay (method described in Fig. 3E, S1, S2). For comparison, we fully synchronized and arrested INA-6 cells at mitosis and released their cell cycle immediately before addition to the hMSC monolayer, rendering them more likely to divide while adhering. Mitotic arrest significantly increased the number of nMA cells and decreased the number of MA cells (Fig. 3F). Furthermore, the nMA population contained significantly more cells cycling in the G_0/G_1 phase than the MA population, both in synchronously and asynchronously cycling INA-6 (Fig. 3G, S3B). The number of nMA INA-6 cells increased due to a higher cell division frequency. Taken together, we showed that INA-6 detach from aggregates by generating one temporarily detached daughter cell after cell division, a process that potentially contributes to the initiation of dissemination.

Well Plate Sandwich Centrifugation (WPSC) Separates hMSC-Interacting INA-6 Subpopulations

To separate nMA and MA cells for further analysis, we developed the method “Well Plate Sandwich Centrifugation” (WPSC), outlined in Fig. 4A. To equalize the background signaling caused by MSC-derived factors and to focus on differences within directly MSC-interacting INA-6 subpopulations, all cultures were incubated in hMSC-conditioned medium (CM) from the respective donors and compared with INA-6 incubation in CM without hMSCs.

Microscopic tracking of nMA and MA INA-6 cell numbers during each WPSC separation step revealed successful separation after the third centrifugation step, whereas CM-treated INA-6 cells required only one centrifugation step (Fig. 4B). Thus, WPSC generated cell numbers that were suitable for subsequent analyses.

RNAseq of non-MSC-Adhering and MSC-Adhering Subpopulations

To characterize the subpopulations separated by WPSC, we conducted RNAseq, revealing 1291 differentially expressed genes between nMA *vs.* CM, 484 between MA *vs.* CM, and 195 between MA *vs.* nMA. We validated RNAseq and found that the differential expression of 18 genes correlated with those measured with qPCR for each pairwise comparison (Fig. 4C-E, S5): nMA *vs.* CM [$\rho(16) = .803$, p = 6.09e-5], MA *vs.* CM [$\rho(16) = .827$, p = 2.30e-5], and MA *vs.* nMA cells [$\rho(16) = .746$, p = 3.74e-4] (Spearman's rank correlation). One of the 18 genes (*MUC1*) measured by qPCR showed a mean expression opposite to that obtained by RNAseq (nMA *vs.* CM), although the difference was insignificant (Fig. 4C). For nMA *vs.* CM, the difference in expression measured by qPCR was significant for only two of the 11 genes (*DKK1* and *OPG*), whereas the other genes (*BCL6*, *BMP4*, *BTG2*, *IL10RB*, *IL24*, *NOTCH2*, *TNFRSF1A*, *TRAF5*) only confirmed the tendency measured by RNAseq (Fig. 4C-E). For MA *vs.* CM, qPCR validated the significant upregulation of seven genes (*TGM2*, *DCN*, *LOX*, *MMP14*, *MMP2*, *CXCL12*, *CXCL8*), whereas the downregulation of *BMP4* was insignificant.

Non-MSC-Adhering INA-6 and MSC-Adhering INA-6 Have Distinct Expression Patterns of Proliferation or Adhesion, Respectively

To functionally characterize the unique transcriptional patterns in nMA-INA6 and MA-INA6, we generated lists of genes that were differentially expressed *vs.* the other two subpopulations [termed nMA *vs.* (MA & CM) and MA *vs.* (nMA & CM)]. Functional enrichment analysis was performed, and the enriched terms were displayed as ontology clusters (Fig. 5A). nMA-INA6 upregulated genes enriched with loosely connected term clusters associated with proliferation (e.g., "positive regulation of cell cycle"). MA-INA6 upregulated genes enriched with tightly connected term clusters related to cell adhesion and the production of ECM factors (e.g. "cell-substrate adhesion"). Similar ontology terms were enriched in the

gene lists obtained from pairwise comparisons (nMA *vs.* CM, MA *vs.* CM, and MA *vs.* nMA) (Fig. 5B). In particular, nMA vs. CM (but not MA vs. CM) upregulated genes that were enriched with “G1/S transition”, showing that WPSC isolated nMA daughter cells after cell division.

To check for similarities between lists of differentially expressed genes from hMSC-interacting subpopulations, we performed enrichment analysis on gene lists from the overlaps (“∩”) between all pairwise comparisons (Fig. 5B, S6), and showed the extent of these overlaps in circos plots (Fig. 5C). The overlap between MA *vs.* CM and nMA *vs.* CM showed neither enrichment with proliferation- nor adhesion-related terms but with apoptosis-related terms. A direct comparison of MSC-interacting subpopulations (MA *vs.* nMA) showed a major overlap with MA *vs.* CM (Fig. 5C, middle). This overlap was enriched with terms related to adhesion but not proliferation. Hence, MA-INA6 and nMA-INA6 mostly differed in their expression of adhesion genes.

To assess whether nMA-INA6 and MA-INA6 were regulated by separate transcription factors, we examined the enrichment of curated regulatory networks from the TRRUST database (Fig. 5B bottom). All the lists were enriched for p53 regulation. E2F1 regulation was observed only in genes upregulated in nMA *vs.* CM and downregulated in MA *vs.* nMA. Genelists involving MA-INA6 were enriched in regulation by subunits of NF-κB (NFKB1/p105 and RELA/p65) and factors of immediate early response (SRF, JUN). Correspondingly, NF-κB and JUN are known to regulate the expression of adhesion factors in multiple myeloma and B-cell lymphoma, respectively (36, 37).

Taken together, MSC-interacting subpopulations showed unique regulatory patterns, focusing on either proliferation or adhesion.

nMA-INA6 and MA-INA6 Show Increased Apoptosis Signaling Mediated by ER-Stress, p53 and Death Domain Receptors

As previously stated, apoptosis rates increased in INA-6 cells grown on confluent hMSCs compared to CM-INA6 cells after 24 h of co-culture (Fig. 1D). Since this setup was similar to that used to separate hMSC-interacting subpopulations using WPSC, we looked for

enrichment of apoptosis-related terms (Fig. 5B). “Regulation of cellular response to stress” and “intrinsic apoptotic signaling pathway (in response to ER-stress)” are terms that were enriched in nMA *vs.* CM, MA *vs.* CM and their overlap. We also found specific stressors for either nMA-INA6 (“intrinsic apoptotic signaling pathway by p53 class mediator”) or MA-INA6 (“extrinsic apoptotic signaling pathway via death domain receptor”). Therefore, apoptosis may be driven by ER stress in both nMA-INA6 and MA-INA6, but also by individual pathways such as p53 and death domain receptors, respectively.

nMA-INA6 and MA-INA6 Regulate Genes Associated with Bone Loss

Myeloma cells cause bone loss by degradation and dysregulation of bone turnover via DKK1 and OPG (38-40). RNAseq of hMSC-interacting subpopulations showed enrichment with functional terms ”skeletal system development” and “ossification” “(Fig. 5A, S6), as well as the regulation of *MMP2*, *MMP14*, *DKK1,* and *OPG*. Validation by qPCR (Fig. 4C, D) showed that MA-INA6 significantly upregulated both *MMP14* and *MMP2* compared with either nMA-INA6 or CM-INA6. The expression of *DKK1*, however, was upregulated significantly in nMA-INA6 (and not significantly upregulated in MA-INA6), while *OPG* was significantly downregulated only in nMA-INA6.

Together, hMSC-interacting subpopulations might contribute to bone loss through different mechanisms: MA-INA6 expression of matrix metalloproteinases and nMA cells via paracrine signaling.

MA-INA6 Upregulate Collagen and Chemokines Associated with Bone Marrow Retention

Retention of myeloma cells within the bone marrow is mediated by adhesion to the ECM (e.g., collagen VI) and the secretion of chemokines (CXCL8 and CXCL12) (7, 11). This directly counteracts dissemination, which is a hallmark of MA-INA6. RNAseq of hMSC-interacting subpopulations showed that genes upregulated in MA-INA6 were enriched with collagen biosynthesis and modifying enzymes, as well as chemotaxis and chemotaxis-related terms (Fig. 5B). Using qPCR, we validated the upregulation of collagen crosslinkers (*LOX* and *TGM2*), collagen-binding *DCN* and chemokines (*CXCL8* and *CXCL12*) in MA-INA6

compared with both nMA-INA6 and CM-INA6 (Fig. 4D). Therefore, MA-INA6 can provide both an adhesive surface and soluble signals for the retention of malignant plasma cells in the bone marrow.

nMA-INA6 Show Highest Viability During IL-6 Withdrawal

Although RNAseq did not reveal IL-6 induction in any WPSC-isolated subpopulation, nMA-INA6 upregulated IGF-1 135%-fold [RNAseq, nMA *vs.* (MA & CM)], which was shown to stimulate growth in CD45+ and IL-6 dependent myeloma cell lines such as INA-6, implying increased autonomy for nMA-INA6 (41).

To test the autonomy of hMSC-interacting INA-6 subpopulations, we isolated them using WPSC after 24 h and 48 h of co-culture, sub-cultured them for 48 h under IL-6 withdrawal, and measured both viability and apoptosis (Fig. 5D). Among the subpopulations, nMA-INA6 was the most viable. Compared to MA-INA6, nMA-INA6 increased cell viability by 8 or 4 fold when co-cultured for 24 or 48 h, respectively [Hedges g of Log_{10}(Fold Change) = 2.31 or 0.82]. However, the difference was no longer significant after 48 h of co-culture, probably because nMA-INA6 adhered to the hMSC layer (turning into MA-INA6) during prolonged co-culture, which could also explain why the viability of MA-INA6 cell subcultures increased with prolonged co-culture. Nevertheless, nMA-INA6 did not achieve the same viability as that of INA-6 cells cultured with IL-6. Despite the differences in viability, subcultures of hMSC-interacting subpopulations did not show any differences in caspase 3/7 activity when co-cultured for 48 h (Fig. 5D, right).

Overall, among the hMSC-interacting subpopulations, nMA-INA6 had the highest chance of surviving IL-6 withdrawal.

Genes Upregulated by MA-INA6 are Associated with an Improved Disease Prognosis

To relate the adhesion of MA-INA6 observed *in vitro* to the progression of multiple myeloma, we assessed patient survival [n = 535, Seckinger et al. 2018 (21, 22) depending on the expression level of 101 genes, which were upregulated in MA *vs.* (nMA & CM) and are part of the ontology terms “Extracellular matrix organization,” “ECM proteoglycans,” “cell-substrate adhesion” and “negative regulation of cell-substrate adhesion” (Fig. 6A, Tab. S2).

As a reference, we generated a list of 173 cell cycle-related genes that were upregulated by nMA-INA6 *vs.* (MA-INA6 & CM-INA6).

As expected, longer patient survival was associated with low expression of the majority of cell cycle genes [71 or 68 genes for progression-free survival (PFS) or overall survival (OS)]. Only a few cell cycle genes (two for PFS and seven for OS) were associated with survival when highly expressed. Intriguingly, adhesion genes showed an inverse pattern: a large group of adhesion genes (24 for PFS and 26 for OS) was significantly associated with improved survival when highly expressed, whereas only a few genes (two for PFS and four for OS) improved survival when expressed at low levels (Tab. 1). We concluded that the myeloma-dependent expression of adhesion factors determined in our *in vitro* study correlates with improved patient survival.

Expression of Adhesion- or Retention-related genes (CXCL12, DCN and TGM2) is Decreased During Progression of Multiple Myeloma

To examine how the disease stage affects the adhesion and bone marrow retention of myeloma cells *in vitro*, we analyzed the expression of *CXCL12* in healthy plasma cell (BMPC) cohorts of patients at different disease stages and in myeloma cell lines (HMCL) [described in Seckinger et al. 2018 (29)] (Fig. 6C). We also included *DCN* and *TGM2* since both are suggested to inhibit metastasis in different cancers by promoting cell-matrix interactions (8, 42). In accordance with independent reports (9, 43), high expression of *CXCL12* and *DCN* by myeloma cells was associated with improved overall survival (adj. p = .009 and .008, respectively) (Fig. 6B).

CXCL12 is expressed by BMPCs (median = 219 normalized counts), but its expression levels are significantly lower from MGUS to relapsed multiple myeloma (MMR) (median = 9 normalized counts in MMR and absent expression in most HMCL). *DCN* (but not *TGM2*) was weakly expressed in BMPCs (Q_1=0.7, Q_3=3.7, normalized counts), whereas *TGM2* was weakly expressed only in patients with monoclonal gammopathy of undetermined significance (MGUS) (Q_1=0.4, Q_3=4.1 normalized counts). The median and upper quartiles of both *DCN*- and *TGM2* decreased continuously after each stage, ending at Q_3=0.9 and

Q_3=0.6, respectively, in MMR. 49 of the 101 adhesion genes (Fig. 6A) followed a similar pattern of continuous downregulation in the advanced stages of multiple myeloma (Fig. S7 and S8), of which 19 genes were associated with longer PFS when they were highly expressed. The other 52 (out of 101) adhesion genes that were not downregulated across disease progression (or were expressed at a level too low to make that categorization) contained only five genes that were associated with longer PFS at high expression (Tab. 1, Tab. S2).

Together, the expression of adhesion or bone marrow retention-related markers (*CXCL12*, *DCN,* and *TGM2)* is reduced or lost at advanced stages of multiple myeloma, which could enhance dissemination and reduce retention in the BM microenvironment.

Discussion

In this study, we developed an *in vitro* model to investigate the attachment/detachment dynamics of INA-6 cells to/from hMSCs and established methods to isolate the attached and detached intermediates nMA-INA6 and MA-INA6. Second, we characterized a cycle of (re)attachment, division, and detachment, linking cell division to the switch that causes myeloma cells to detach from hMSC adhesion (Fig. 7). Thirdly, we identified clinically relevant genes associated with patient survival, in which better or worse survival was based on the adherence status of INA-6 to hMSCs.

INA-6 cells emerged as a robust choice for studying myeloma dissemination *in vitro*, showing rapid and strong adherence, as well as aggregation exceeding MSC saturation. The IL-6 dependency of INA-6 enhanced the resemblance of myeloma cell lines to patient samples, with INA-6 ranking 13th among 66 cell lines (44). Despite variations in bone marrow MSCs between multiple myeloma (MM) and healthy states, we anticipated the robustness of our results, given the persistent strong adherence and growth signaling from MSCs to INA-6 during co-cultures (45).

We acknowledge that INA-6 cells alone cannot fully represent the complexity of myeloma aggregation and detachment dynamics. However, the diverse adhesive properties of myeloma cell lines pose a challenge. We reasoned that attempting to capture this complexity

within a single publication would not be possible. Our focus on INA-6 interactions with hMSCs allowed for a detailed exploration of the observed phenomena, such as the unique aggregation capabilities that facilitate the easy detection of detaching cells *in vitro*. The validity of our data was demonstrated by matching the *in vitro* findings with the gene expression and survival data of the patients (e.g. CXCL12, DCN, and TGM2 expression, n=873), ensuring biological consistency and generalizability regardless of the cell line used.

The protocols presented in this study offer a cost-efficient and convenient solution, making them potentially valuable for a broader study of cell interactions. We encourage optimizations to meet the varied adhesive properties of the samples, such as decreasing the number of washing steps if the adhesive strength is low. We caution against strategies that average over multiple cell lines without prior understanding their diverse attachment/detachment dynamics, such as homotypic aggregation. Such detailed insights may prove instrumental when considering the diversity of myeloma patient samples across different disease stages (34, 35).

The intermediates, nMA-INA6 and MA-INA6, were distinct but shared similarities in response to cell stress, intrinsic apoptosis, and regulation by p53. Unique regulatory patterns were related to central transcription factors: E2F1 for nMA-INA6; and NF-κB, SRF, and JUN for MA-INA6. This distinction may have been established through antagonism between p53 and the NF-κB subunit RELA/p65 (46, 47). Similar regulatory patterns were found in transwell experiments with RPMI1-8226 myeloma cells, where direct contact with the MSC cell line HS5 led to NF-κB signaling and soluble factors to E2F signaling (20).

The first subpopulation, nMA-INA6, represented proliferative and disseminative cells; nMA-INA6 drove detachment through cell division, which was regulated by E2F, p53, and likely their crosstalk (48). They upregulate cell cycle progression genes associated with worse prognosis, because proliferation is a general risk factor for an aggressive disease course (49). Additionally, nMA-INA6 survived IL-6 withdrawal better than CM-INA6 and MA-INA6, implying their ability to proliferate independently of the bone marrow (1). Indeed, xenografted INA-6 cells developed autocrine IL-6 signaling but remained IL-6-dependent after

explantation (23). The increased autonomy of nMA-INA6 cells can be explained by the upregulation of IGF-1, being the major growth factor for myeloma cell lines (41). Other reports characterized disseminating cells differently: Unlike nMA-INA6, circulating myeloma tumor cells were reported to be non-proliferative and bone marrow retentive (50). In contrast to circulating myeloma tumor cells, nMA-INA6 were isolated shortly after detachment and therefore these cells are not representative of further steps of dissemination, such as intravasation, circulation or intravascular arrest (3). Furthermore, Brandl et al. described proliferative and disseminative myeloma cells as separate entities, depending on the surface expression of CD138 or JAM-C (4, 51). Although CD138 was not differentially regulated in nMA-INA6 or MA-INA6, both subpopulations upregulated JAM-C, indicating disease progression (51).

Furthermore, nMA-INA6 showed that cell division directly contributed to dissemination. This was because INA-6 daughter cells emerged from the mother cell with distance to the hMSC plane in the 2D setup. A similar mechanism was described in an intravasation model in which tumor cells disrupt the vessel endothelium through cell division and detach into blood circulation (52). Overall, cell division offers key mechanistic insights into dissemination and metastasis.

The other subpopulation, MA-INA6, represented cells retained in the bone marrow; MA-INA6 strongly adhered to MSCs, showed NF-κB signaling, and upregulated several retention, adhesion, and ECM factors. The production of ECM-associated factors has recently been described in MM.1S and RPMI-8226 myeloma cells (53). Another report did not identify the upregulation of such factors after direct contact with the MSC cell line HS5; hence, primary hMSCs may be crucial for studying myeloma-MSC interactions (20). Moreover, MA-INA6 upregulated adhesion genes associated with prolonged patient survival and showed decreased expression in relapsed myeloma. As myeloma progression implies the independence of myeloma cells from the bone marrow (1, 44), we interpreted these adhesion genes as mediators of bone marrow retention, decreasing the risk for dissemination and thereby potentially prolonging patient survival. However, the overall impact of cell adhesion

and ECM on patient survival remains unclear. Several adhesion factors have been proposed as potential therapeutic targets (51, 54). Recent studies have described the prognostic value of multiple ECM genes, such as those driven by NOTCH (53). Another study focused on ECM gene families, of which only six of the 26 genes overlapped with our gene set (Tab. S2) (55). The expression of only one gene (*COL4A1*) showed a different association with overall survival than that in our cohort. The lack of overlap and differences can be explained by dissimilar definitions of gene sets (homology *vs.* gene ontology), methodological discrepancies, and cohort composition.

In summary, our *in vitro* model provides a starting point for understanding the initiation of dissemination and its implications for patient survival, providing innovative methods, mechanistic insights into attachment/detachment, and a set of clinically relevant genes that play a role in bone marrow retention. These results and methods might prove useful when facing the heterogeneity of disseminative behaviors among myeloma cell lines and primary materials.

Acknowledgements

This work was supported by the Deutsche Forschungsgemeinschaft (DFG) SPP microBONE grants EB 447/10-1 (491715122), JA 504/17-1, HO 4462/1-1 (401358321), JU 426/10-1 (491715122), and JU 426/11-1 (496963451). MH was funded by the IZKF project D-361, and EL was funded by Deutsche Krebshilfe (70112693) and Wilhelm Sander-Stiftung (2014.903.1). We thank the Core Unit Systemmedizin (SysMed), c/o Institut für Molekulare Infektionsbiologie (IMIB), University of Würzburg for performing the RNAseq analyses, as well as the Elite Netzwerk Bayern and the Graduate School of Life Sciences of the University of Würzburg.

References

1. Bladé J, Beksac M, Caers J, Jurczyszyn A, von Lilienfeld-Toal M, Moreau P, et al. Extramedullary disease in multiple myeloma: a systematic literature review. Blood Cancer Journal. 2022;12(3):1-10.

2. Rajkumar SV, Dimopoulos MA, Palumbo A, Blade J, Merlini G, Mateos M-V, et al. International Myeloma Working Group updated criteria for the diagnosis of multiple myeloma. The Lancet Oncology. 2014;15(12):e538-48.

3. Zeissig MN, Zannettino ACW, Vandyke K. Tumour Dissemination in Multiple Myeloma Disease Progression and Relapse: A Potential Therapeutic Target in High-Risk Myeloma. Cancers (Basel). 2020;12(12).

4. Akhmetzyanova I, McCarron MJ, Parekh S, Chesi M, Bergsagel PL, Fooksman DR. Dynamic CD138 surface expression regulates switch between myeloma growth and dissemination. Leukemia. 2020;34(1):245-56.

5. Garcia-Ortiz A, Rodriguez-Garcia Y, Encinas J, Maroto-Martin E, Castellano E, Teixido J, et al. The Role of Tumor Microenvironment in Multiple Myeloma Development and Progression. Cancers (Basel). 2021;13(2).

6. Aggarwal R, Ghobrial IM, Roodman GD. Chemokines in multiple myeloma. Experimental hematology. 2006;34(10):1289-95.

7. Alsayed Y, Ngo H, Runnels J, Leleu X, Singha UK, Pitsillides CM, et al. Mechanisms of regulation of CXCR4/SDF-1 (CXCL12)-dependent migration and homing in multiple myeloma. Blood. 2007;109(7):2708-17.

8. Hu X, Villodre ES, Larson R, Rahal OM, Wang X, Gong Y, et al. Decorin-mediated suppression of tumorigenesis, invasion, and metastasis in inflammatory breast cancer. Communications Biology. 2021;4(1):72.

9. Huang S-Y, Lin H-H, Yao M, Tang J-L, Wu S-J, Hou H-A, et al. Higher Decorin Levels in Bone Marrow Plasma Are Associated with Superior Treatment Response to Novel Agent-Based Induction in Patients with Newly Diagnosed Myeloma - A Retrospective Study. PloS One. 2015;10(9):e0137552.

10. Katz B-Z. Adhesion molecules—The lifelines of multiple myeloma cells. Seminars in Cancer Biology. 2010;20(3):186-95.

11. Kibler C, Schermutzki F, Waller HD, Timpl R, Müller CA, Klein G. Adhesive interactions of human multiple myeloma cell lines with different extracellular matrix molecules. Cell Adhesion and Communication. 1998;5(4):307-23.

12. Glavey SV, Naba A, Manier S, Clauser K, Tahri S, Park J, et al. Proteomic characterization of human multiple myeloma bone marrow extracellular matrix. Leukemia. 2017;31(11):2426-34.

13. Sanz-Rodríguez F, Ruiz-Velasco N, Pascual-Salcedo D, Teixidó J. Characterization of VLA-4-dependent myeloma cell adhesion to fibronectin and VCAM-1: VLA-4-dependent Myeloma Cell Adhesion. British Journal of Haematology. 1999;107(4):825-34.

14. Chatterjee M, Hönemann D, Lentzsch S, Bommert K, Sers C, Herrmann P, et al. In the presence of bone marrow stromal cells human multiple myeloma cells become independent of the IL-6/gp130/STAT3 pathway. Blood. 2002;100(9):3311-8.

15. Hideshima T, Mitsiades C, Tonon G, Richardson PG, Anderson KC. Understanding multiple myeloma pathogenesis in the bone marrow to identify new therapeutic targets. Nature Reviews Cancer. 2007;7(8):585-98.

16. Frassanito MA, Cusmai A, Iodice G, Dammacco F. Autocrine interleukin-6 production and highly malignant multiple myeloma: relation with resistance to drug-induced apoptosis. Blood. 2001;97(2):483-9.

17. Urashima M, Chauhan D, Uchiyama H, Freeman G, Anderson K. CD40 ligand triggered interleukin-6 secretion in multiple myeloma. Blood. 1995;85(7):1903-12.

18. Solimando AG, Malerba E, Leone P, Prete M, Terragna C, Cavo M, et al. Drug resistance in multiple myeloma: Soldiers and weapons in the bone marrow niche. Frontiers in Oncology. 2022;12:973836.

19. Ghobrial IM. Myeloma as a model for the process of metastasis: implications for therapy. Blood. 2012;120(1):20-30.

20. Dziadowicz SA, Wang L, Akhter H, Aesoph D, Sharma T, Adjeroh DA, et al. Bone Marrow Stroma-Induced Transcriptome and Regulome Signatures of Multiple Myeloma. Cancers. 2022;14(4):927.

21. Seckinger A, Delgado JA, Moser S, Moreno L, Neuber B, Grab A, et al. Target Expression, Generation, Preclinical Activity, and Pharmacokinetics of the BCMA-T Cell Bispecific Antibody EM801 for Multiple Myeloma Treatment. Cancer Cell. 2017;31(3):396-410.

22. Seckinger A, Hillengass J, Emde M, Beck S, Kimmich C, Dittrich T, et al. CD38 as Immunotherapeutic Target in Light Chain Amyloidosis and Multiple Myeloma-Association With Molecular Entities, Risk, Survival, and Mechanisms of Upfront Resistance. Frontiers in Immunology. 2018;9:1676.

23. Burger R, Guenther A, Bakker F, Schmalzing M, Bernand S, Baum W, et al. Gp130 and ras mediated signaling in human plasma cell line INA-6: a cytokine-regulated tumor model for plasmacytoma. The Hematology Journal: The Official Journal of the European Haematology Association. 2001;2(1):42-53.

24. Gramatzki M, Burger R, Trautman U, Marschalek R, Lorenz H, Hansen-Hagge TE, et al. Two new interleukin-6 dependent plasma cell lines carrying a chromosomal abnormality involving the IL-6 gene locus. 1994;84 Suppl. 1:173a-a.

25. Anders S, Pyl PT, Huber W. HTSeq--a Python framework to work with high-throughput sequencing data. Bioinformatics (Oxford, England). 2015;31(2):166-9.

26. Dobin A, Davis CA, Schlesinger F, Drenkow J, Zaleski C, Jha S, et al. STAR: ultrafast universal RNA-seq aligner. Bioinformatics. 2013;29(1):15-21.

27. Zerbino DR, Achuthan P, Akanni W, Amode M R, Barrell D, Bhai J, et al. Ensembl 2018. Nucleic Acids Research. 2018;46(D1):D754-D61.

28. Zhou Y, Zhou B, Pache L, Chang M, Khodabakhshi AH, Tanaseichuk O, et al. Metascape provides a biologist-oriented resource for the analysis of systems-level datasets. Nature Communications. 2019;10(1):1523.

624 29. Seabold S, Perktold J, editors. Statsmodels: Econometric and statistical modeling
625 with python. Proceedings of the 9th Python in Science Conference; 2010: Austin, TX.
626 30. Vallat R. Pingouin: statistics in Python. Journal of Open Source Software.
627 2018;3(31):1026.
628 31. Kuric M, Ebert R. plotastic: Bridging Plotting and Statistics in Python. The Journal of
629 Open Source Software. 2024.
630 32. Hothorn T, Lausen B. Maximally Selected Rank Statistics in R. R News. 2002;2:3-5.
631 33. Kuric M, Ebert R. markur4/Supplemental-INA-6-Subpopulations-and-Aggregation-
632 Detachment-Dynamics: Supplementary Data [
633 34. Kawano MM, Huang N, Tanaka H, Ishikawa H, Sakai A, Tanabe O, et al. Homotypic
634 cell aggregations of human myeloma cells with ICAM-1 and LFA-1 molecules. British Journal
635 of Haematology. 1991;79(4):583-8.
636 35. Okuno Y, Takahashi T, Suzuki A, Ichiba S, Nakamura K, Okada T, et al. In vitro
637 growth pattern of myeloma cells in liquid suspension or semi-solid culture containing
638 interleukin-6. International Journal of Hematology. 1991;54(1):41-7.
639 36. Blonska M, Zhu Y, Chuang HH, You MJ, Kunkalla K, Vega F, et al. Jun-regulated
640 genes promote interaction of diffuse large B-cell lymphoma with the microenvironment.
641 Blood. 2015;125(6):981-91.
642 37. Tai Y-T, Li X-F, Breitkreutz I, Song W, Neri P, Catley L, et al. Role of B-cell-activating
643 factor in adhesion and growth of human multiple myeloma cells in the bone marrow
644 microenvironment. Cancer Research. 2006;66(13):6675-82.
645 38. Standal T, Seidel C, Plesner T, Sanderson R, Waage A, Børset M, et al.
646 Osteoprotegerin is bound, internalized, and degraded by multiple myeloma cells. Blood.
647 2002;100:3002-7.
648 39. Van Valckenborgh E, Croucher PI, De Raeve H, Carron C, De Leenheer E, Blacher
649 S, et al. Multifunctional role of matrix metalloproteinases in multiple myeloma: a study in the
650 5T2MM mouse model. Am J Pathol. 2004;165(3):869-78.

651 40. Zhou F, Meng S, Song H, Claret FX. Dickkopf-1 is a key regulator of myeloma bone
652 disease: opportunities and challenges for therapeutic intervention. Blood reviews.
653 2013;27(6):261-7.
654 41. Sprynski AC, Hose D, Caillot L, Rème T, Shaughnessy JD, Barlogie B, et al. The role
655 of IGF-1 as a major growth factor for myeloma cell lines and the prognostic relevance of the
656 expression of its receptor. Blood. 2009;113(19):4614-26.
657 42. Tabolacci C, De Martino A, Mischiati C, Feriotto G, Beninati S. The Role of Tissue
658 Transglutaminase in Cancer Cell Initiation, Survival and Progression. Medical Sciences.
659 2019;7(2):19.
660 43. Bao L, Lai Y, Liu Y, Qin Y, Zhao X, Lu X, et al. CXCR4 is a good survival prognostic
661 indicator in multiple myeloma patients. Leukemia Research. 2013;37(9):1083-8.
662 44. Sarin V, Yu K, Ferguson ID, Gugliemini O, Nix MA, Hann B, et al. Evaluating the
663 efficacy of multiple myeloma cell lines as models for patient tumors via transcriptomic
664 correlation analysis. Leukemia. 2020;34(10):2754-65.
665 45. Dotterweich J, Schlegelmilch K, Keller A, Geyer B, Schneider D, Zeck S, et al.
666 Contact of myeloma cells induces a characteristic transcriptome signature in skeletal
667 precursor cells -Implications for myeloma bone disease. Bone. 2016;93:155-66.
668 46. Wadgaonkar R, Phelps KM, Haque Z, Williams AJ, Silverman ES, Collins T. CREB-
669 binding protein is a nuclear integrator of nuclear factor-kappaB and p53 signaling. The
670 Journal of Biological Chemistry. 1999;274(4):1879-82.
671 47. Webster GA, Perkins ND. Transcriptional Cross Talk between NF-κB and p53.
672 Molecular and Cellular Biology. 1999;19(5):3485-95.
673 48. Polager S, Ginsberg D. p53 and E2f: partners in life and death. Nature Reviews
674 Cancer. 2009;9(10):738-48.
675 49. Hose D, Rème T, Hielscher T, Moreaux J, Messner T, Seckinger A, et al. Proliferation
676 is a central independent prognostic factor and target for personalized and risk-adapted
677 treatment in multiple myeloma. Haematologica. 2011;96(1):87-95.

50. Garcés J-J, Simicek M, Vicari M, Brozova L, Burgos L, Bezdekova R, et al. Transcriptional profiling of circulating tumor cells in multiple myeloma: a new model to understand disease dissemination. Leukemia. 2020;34(2):589-603.

51. Brandl A, Solimando AG, Mokhtari Z, Tabares P, Medler J, Manz H, et al. Junctional adhesion molecule C expression specifies a CD138low/neg multiple myeloma cell population in mice and humans. Blood Advances. 2022;6(7):2195-206.

52. Wong AD, Searson PC. Mitosis-mediated intravasation in a tissue-engineered tumor-microvessel platform. Cancer research. 2017;77(22):6453-61.

53. Maichl DS, Kirner JA, Beck S, Cheng W-H, Krug M, Kuric M, et al. Identification of NOTCH-driven matrisome-associated genes as prognostic indicators of multiple myeloma patient survival. Blood Cancer Journal. 2023;13(1):1-6.

54. Bou Zerdan M, Nasr L, Kassab J, Saba L, Ghossein M, Yaghi M, et al. Adhesion molecules in multiple myeloma oncogenesis and targeted therapy. International Journal of Hematologic Oncology. 2022;11(2):IJH39.

55. Evers M, Schreder M, Stühmer T, Jundt F, Ebert R, Hartmann TN, et al. Prognostic value of extracellular matrix gene mutations and expression in multiple myeloma. Blood Cancer Journal. 2023;13(1):43.

Figure Legends

Fig. 1: INA-6 growth conformations and survival on hMSCs. **A:** Interaction of INA-6 (green) with hMSCs (black, negative staining) at different INA-6 densities (constant hMSC densities). Scale bar = 200 µm. **B:** Frequency of single hMSCs (same as A) that are covered by INA-6 of varying group sizes. Technical replicates = three per datapoint; Single hMSCs evaluated: 100 per technical replicate. **C:** Interaction of INA-6 with hMSCs at different hMSC densities (constant INA-6 densities). Scale bar = 300 µm. **D:** Two types of homotypic interaction: Attachment after cell contact and sustained attachment of daughter cells after cell division. Datapoints represent one of four independent time-lapse recordings, each evaluating 116 interaction events. **E:** Effects of hMSC-density on the viability (ATP, top) and apoptosis (Caspase3/7 activity, bottom). INA-6:MSC ratio = 4:1; Technical replicates = four per datapoint; **E left:** Signals were measured in INA-6 washed off from hMSCs and normalized by INA-6 cultured in MSC-conditioned medium (= red line) (n=4). **E right:** Signals were measured in co-cultures and normalized by the sum of the signals measured in hMSC and INA-6 cultured separately (= red line) (n=3). **Statistics:** Paired t-test, two-factor RM-ANOVA. Datapoints represent independent co-cultures with hMSCs from three (A, B, D, E right), four (E left) unique donors. Confl. = Confluent.

Fig. 2: Time-lapse analysis of INA-6 detachment from INA-6 aggregates and hMSCs. **A:** Frequency of observed INA-6 aggregates that did or did not lose INA-6 cell(s). 87 aggregates were evaluated per datapoint. **B:** Example of an “disseminating” INA-6 aggregate growing on fluorescently (PKH26) stained hMSC (from A-D). Dashed green lines are trajectories of detached INA-6 cells. Scale bar = 50 µm. **(C-E):** Quantitative assessment of INA-6 detachments. 45 detachment events were evaluated per datapoint. Seeding ratio INA-6:MSC = 4:1. **C:** Most INA-6 cells dissociated from another INA-6 cell and not from an hMSC [$F(1, 3) = 298$, p-unc=4.2e-4]. **D:** Detachment frequency of aggregate size categories. **E:** Detachment frequency of INA-6 cells detaching as single, pairs or more than three cells. **Statistics:** (A): Paired-t-test; (C-E): Paired-t-test, Two-factor RM-ANOVA; Datapoints

represent three (A) or four (C-E) independent time-lapse recordings of co-cultures with hMSCs from two (A) or three (C-E) unique donors.

Fig. 3: Detachment of INA-6 daughter cells after Cell Division. **(A-D):** INA-6 divisions in interaction with confluent hMSCs. Seeding ratio INA-6:MSC = 4:20. **A:** Three examples of dividing INA-6 cells generating either two MA, or one MA and one nMA daughter cells as described in (G). Dashed circles mark mother cells (white), MA cell (blue), and first position of nMA cell (green). Scale bar: 20 µm. **B:** Cell division of MSC-adhering (MA) mother cell can yield one mobile non-MSC-adhering (nMA) daughter cell. **C:** Frequencies of INA-6 pairs defined in (A, B) per observed cell division. 65 divisions were evaluated for each of three independent time-lapse recordings. **D:** Rolling duration of nMA cells after division did not depend on hMSC donor [H(2) = 5.250, p-unc = .072]. Datapoints represent single nMA-cells after division. **(E-G):** Adhesive and cell cycle assessment of MSC-interacting INA-6 subpopulations using the V-Well assay. **E:** Schematic of V-Well Assay (See Fig. S1 for detailed analysis). MSC-interacting subpopulations were separated by subsequent centrifugation and removal of the pellet. The pellet size was quantified by its total fluorescence brightness. Adhering subpopulations were resuspended by rough pipetting. **F:** Relative cell pellet sizes of adhesive INA-6 subpopulations that cycle either asynchronously or were synchronized at mitosis. Gray lines in-between points connect dependent measurements of co-cultures (n=9) that shared the same hMSC-donor and INA-6 culture. Co-cultures were incubated for three different durations (1 h, 2 h, and 3 h after INA-6 addition). Time points were pooled, since time did not show an effect on cell adhesion [F(2,4) = 1.414, p-unc = 0.343]. Factorial RM-ANOVA shows an interaction between cell cycle and the kind of adhesive subpopulation [F(1, 8) = 42.67, p-unc = 1.82e-04]. Technical replicates = 4 per datapoint. **G:** Cell cycles were profiled in cells gathered from the pellets of four independent co-cultures (n=4) and the frequency of G0/G1 cells are displayed depending on co-culture duration (see Fig. S3 for cell cycle profiles). Four Technical replicates were pooled after pelleting. **Statistics:** (D): Kruskal-Wallis H-test. (F): Paired t-test,

(G): Paired t-test, two-factor RM-ANOVA. Datapoints represent INA-6 from independent co-cultures with hMSCs from three unique donors.

Fig. 4: Separation and gene expression of INA-6 subpopulations. **A:** Schematic of “Well-Plate Sandwich Centrifugation” (WPSC) separating nMA- from MA-INA6. A co-culture 96 well plate is turned upside down and attached on top of a “catching plate”, forming a “well-plate sandwich”. nMA-INA6 cells are collected in the catching plate by subsequent rounds of centrifugation and gentle washing. MA-INA6 are enzymatically dissociated from hMSCs or by rough pipetting. Subsequent RNAseq of MSC-interacting subpopulations reveals distinct expression clusters [right, multidimensional scaling plot (MDS) (n=5)]. **B:** Separation was microscopically tracked after each centrifugation step. **(C-E):** RT-qPCR of genes derived from RNAseq results. Expression was normalized to the median of CM-INA6. Samples include those used for RNAseq and six further co-cultures (n=11; non-detects were discarded). **C:** Adhesion factors, ECM proteins and matrix metalloproteinases. **D:** Factors involved in bone remodeling and bone homing chemokines. **E:** Factors involved in (immune) signaling. **Statistics**: (C-E): Paired t-test. Datapoints represent the mean of three (B-E) technical replicates. INA-6 were isolated from independent co-cultures with hMSCs from five (A, B), nine (C-E) unique donors.

Fig. 5: Functional analysis of MSC-interacting subpopulations **(A-C):** Functional enrichment analysis of differentially expressed genes (from RNAseq) using Metascape. **A:** Gene ontology (GO) cluster analysis of gene lists that are unique for MA (left) or nMA (right) INA-6. Circle nodes represent subsets of input genes falling into similar GO-term. Node size grows with the number of input genes. Node color defines a shared parent GO-term. Two nodes with a similarity score > 0.3 are linked. **B:** Enrichment analysis of pairwise comparisons between MA subpopulations and their overlaps (arranged in columns). GO terms were manually picked and categorized (arranged in rows). Raw Metascape results are shown in Fig. S6. For each GO-term, the p-values (x-axis) and the counts of matching input genes

(circle size) were plotted. The lowest row shows enrichment of gene lists from the TRRUST-database. **C:** Circos plots by Metascape. Sections of a circle represent lists of differentially expressed genes. Purple lines connect same genes appearing in two gene lists. ∩: Overlapping groups, MA: MSC-adhering, nMA: non-MSC-adhering, CM: MSC-Conditioned Medium. **D:** INA-6 were co-cultured on confluent hMSC for 24 h or 48 h, separated by WPSC and sub-cultured for 48 h under IL-6 withdrawal (n=6), except the control (IL-6 + INA-6) (n=3). Signals were normalized (red line) to INA-6 cells grown without hMSCs and IL-6 (n=3). Statistics (D): Paired t-test, two-factor RM-ANOVA. Datapoints represent the mean of four technical replicates. INA-6 were isolated from independent co-cultures with hMSCs from six unique donors.

Fig. 6: Survival of patients with multiple myeloma regarding the expression levels of adhesion and bone retention genes. **A:** p-value distribution of genes associated with patient survival (n=535) depending on high or low expression levels. Red dashed line marks the significance threshold of p-adj=0.05. Histogram of p-values was plotted using a bin width of -log10(0.05)/2. Patients with high and low gene expression were delineated using maximally selected rank statistics (maxstat). **B:** Survival curves for three genes taken from the list of adhesion genes shown in (A), maxstat thresholds defining high and low expression were: CXCL12: 81.08; DCN: 0.75; TGM2: 0.66 normalized counts. **C:** Gene expression (RNAseq, n = 873) measured in normalized counts (edgeR) of CXCL12, DCN in Bone Marrow Plasma Cell (BMPC), Monoclonal Gammopathy of Undetermined Significance (MGUS), smoldering Multiple Myeloma (sMM), Multiple Myeloma (MM), Multiple Myeloma Relapse (MMR), Human Myeloma Cell Lines (HMCL). The red dashed line marks one normalized read count. **Statistics** (A, B): Log-rank test; (C): Kruskal-Wallis, Mann–Whitney U Test. All p-values were corrected using the Benjamini-Hochberg procedure.

Fig. 7: Proposed model of “Detached Daughter Driven Dissemination” (DDDD) in aggregating multiple myeloma. **Heterotypic Interaction:** Malignant plasma cells colonize the

bone marrow microenvironment by adhering to an MSC (or osteoblast, ECM, etc.) to maximize growth and survival through paracrine and adhesion mediated signaling, even if contact may trigger initial apoptosis. Gene expression will focus on establishing a strong anchor within the bone marrow, but also on attracting other myeloma cells (via secretion of ECM factors and CXCL12/CXCL8, respectively). **Cell Division:** Cell fission can generate one daughter cell that no longer adheres to the MSC (nMA). **Homotypic Interaction:** If myeloma cells have the capacity to grow as aggregates, the daughter cell stays attached to their MSC-adhering mother cell (MA). **Re-Adhesion:** The daughter cell "rolls around" the mother cell until it re-adheres to the MSC. Our model estimates the rolling duration to be 1-10 h long. **Proliferation & Saturation:** We estimate that a single myeloma cell covers one MSC completely after roughly four population doublings. When heterotypic adhesion is saturated, subsequent daughter cells benefit from a homotypic interaction, since they stay close to growth-factor secreting MSCs and focus gene expression on proliferation (e.g. driven by E2F) and not adhesion (driven by NF-κB). **Critical Size:** Homotypic interaction is weaker than heterotypic interaction, and each cell fission destabilizes the aggregate. Hence, detachment of myeloma cells may depend mostly on aggregate size. **Dissemination:** After myeloma cells have detached, they gained a viability advantage through IL-6-independence (with unknown duration), which enhances their survival outside of the bone marrow and allows them to spread throughout the body.

Tab 1: Adhesion and ECM genes (shown in Fig. 6A) were filtered by their association with patient survival (p-adj. < 0.01) and was categorized as continuous downregulation during disease progression. The complete list is presented in Table S2. Bone Marrow Plasma Cells (BMPC), Monoclonal Gammopathy of Undetermined Significance (MGUS), moldering Multiple Myeloma (sMM), Multiple Myeloma (MM), and Multiple Myeloma Relapse (MMR). p-unc = unadjusted p-values; p-adj: p-values adjusted using the Benjamini-Hochberg method with 101 genes.

838 Fig. 1

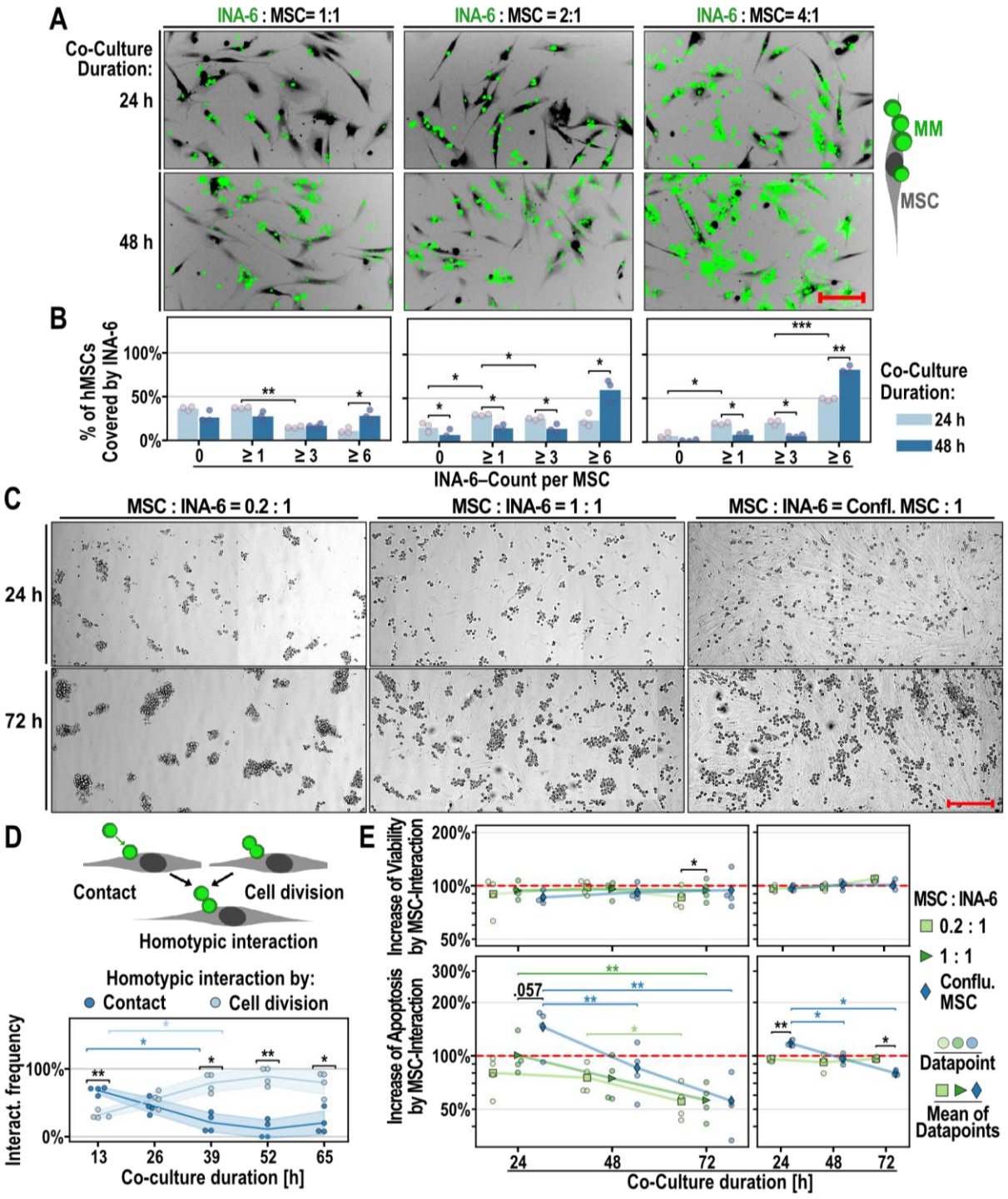

839

840

841 Fig. 2

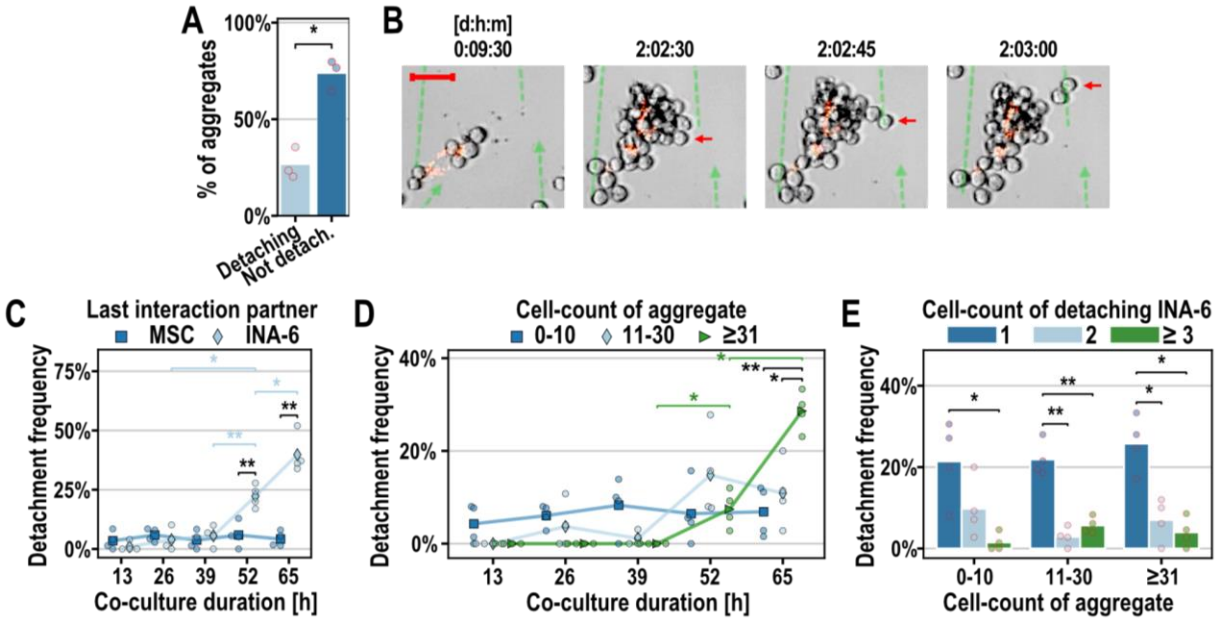

842

843

844 Fig. 3

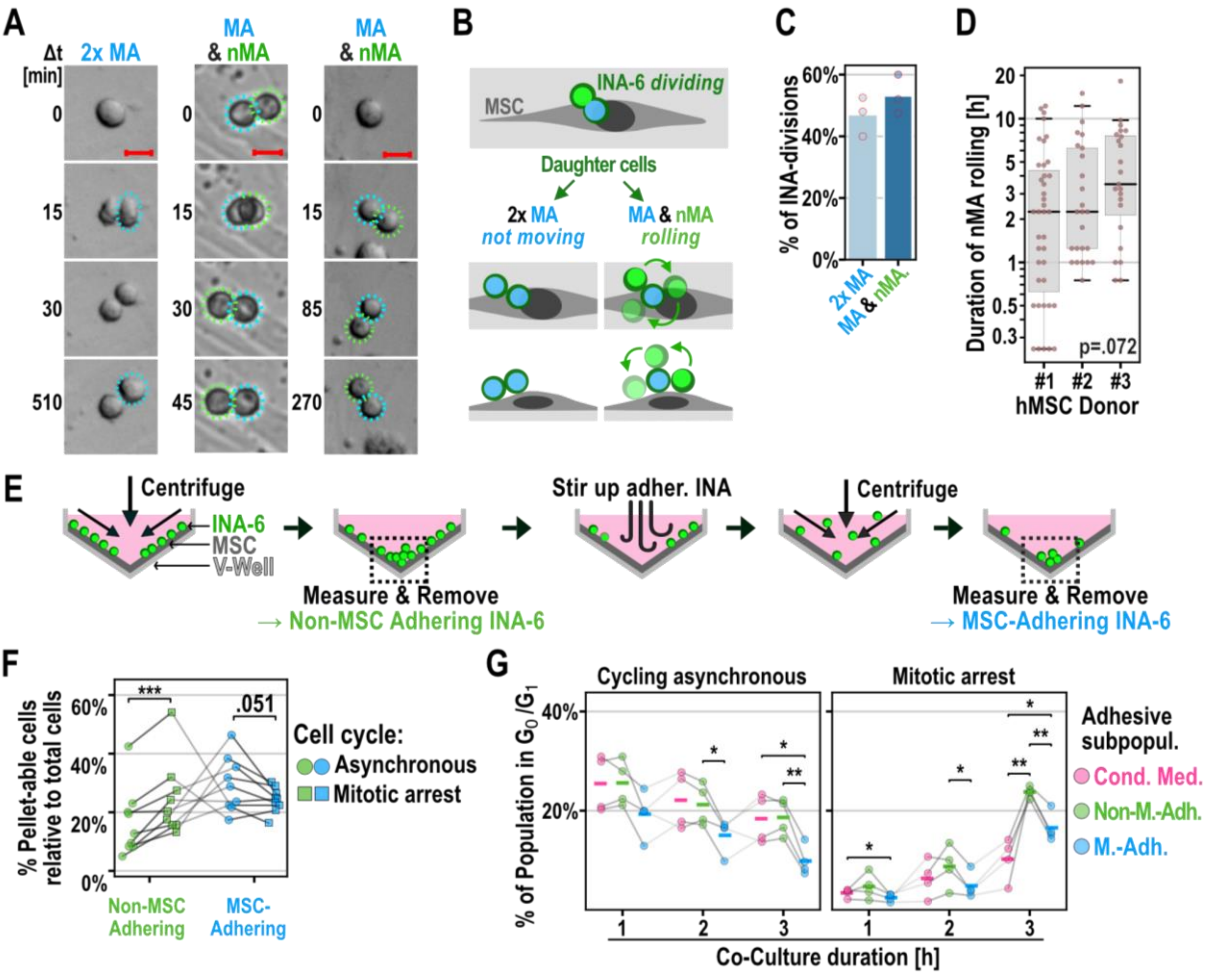

845

846

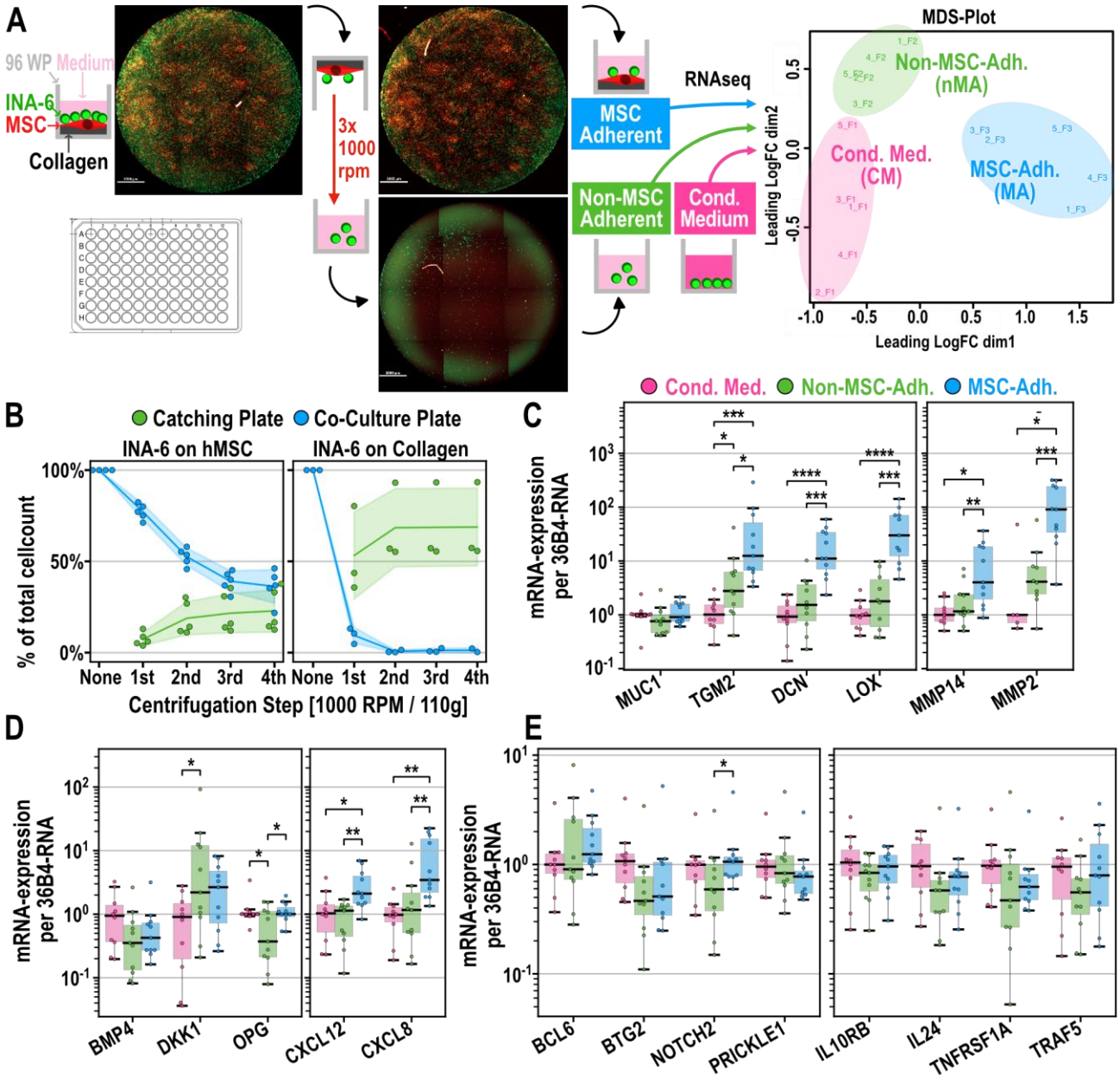
A
96 WP Medium
INA-6
MSC
Collagen
3x
1000
rpm
RNAseq
MSC
Adherent
Non-MSC
Adherent
Cond.
Medium
MDS-Plot
Non-MSC-Adh.
(nMA)
Cond. Med.
(CM)
MSC-Adh.
(MA)
Leading LogFC dim2
Leading LogFC dim1
B
Catching Plate
Co-Culture Plate
INA-6 on hMSC
INA-6 on Collagen
% of total cellcount
100%
50%
0%
None 1st 2nd 3rd 4th
Centrifugation Step [1000 RPM / 110g]
C
Cond. Med.
Non-MSC-Adh.
MSC-Adh.
mRNA-expression
per 36B4-RNA
MUC1
TGM2
DCN
LOX
MMP14
MMP2
D
BMP4
DKK1
OPG
CXCL12
CXCL8
E
BCL6
BTG2
NOTCH2
PRICKLE1
IL10RB
IL24
TNFRSF1A
TRAF5

847 Fig. 4

848 Fig. 5

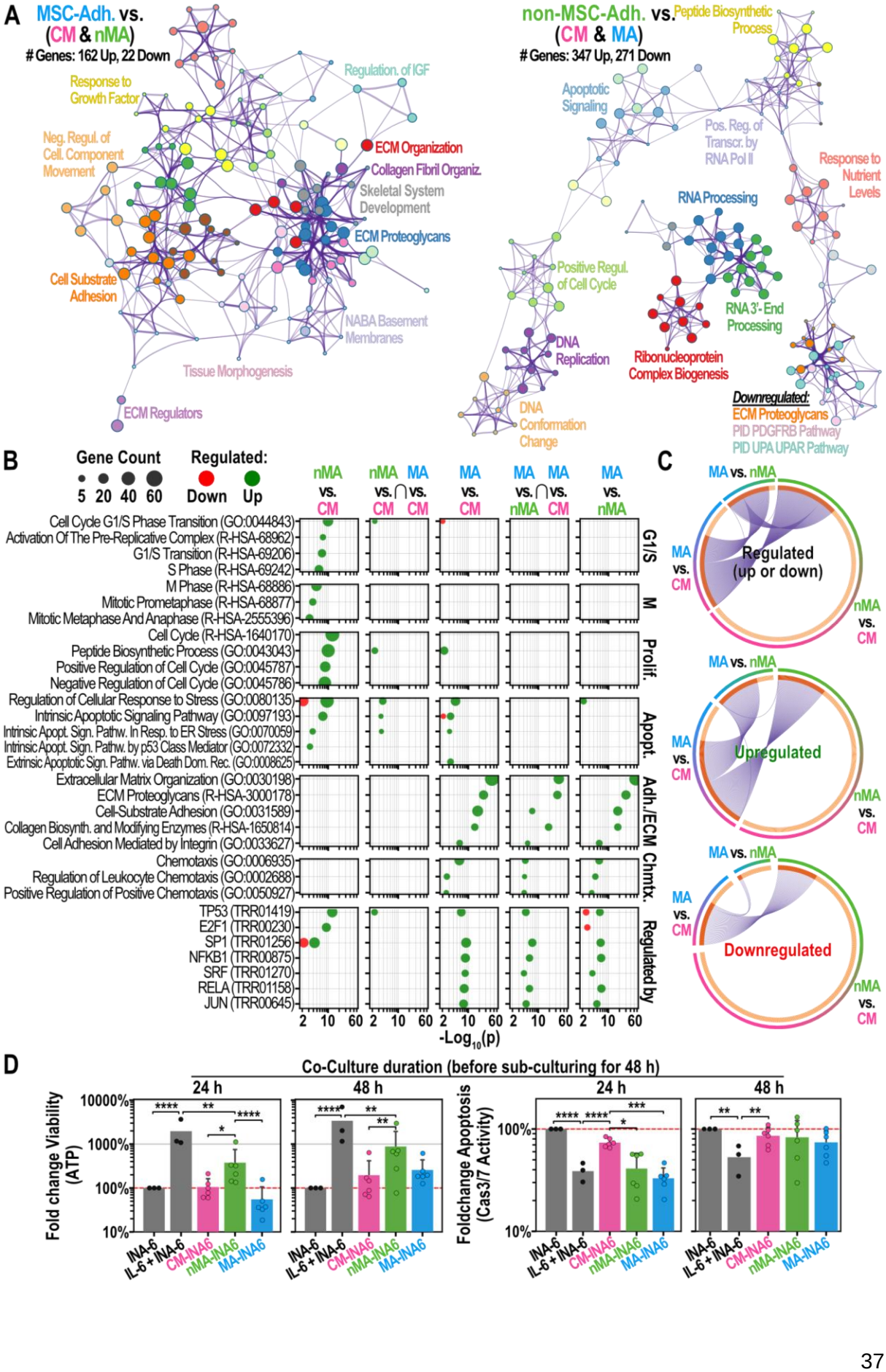

849
850

851 Fig. 6

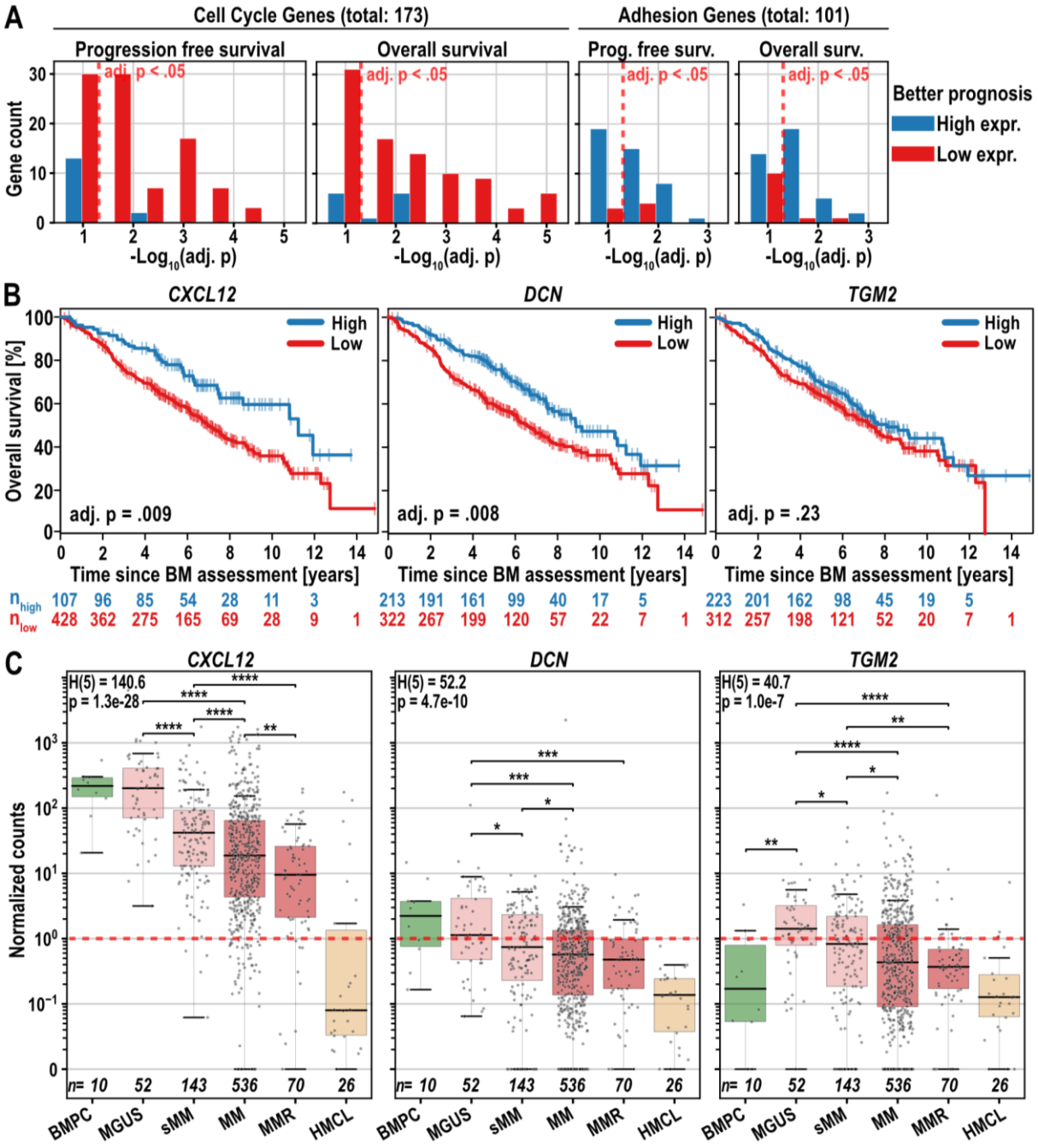

852
853

854 Fig. 7

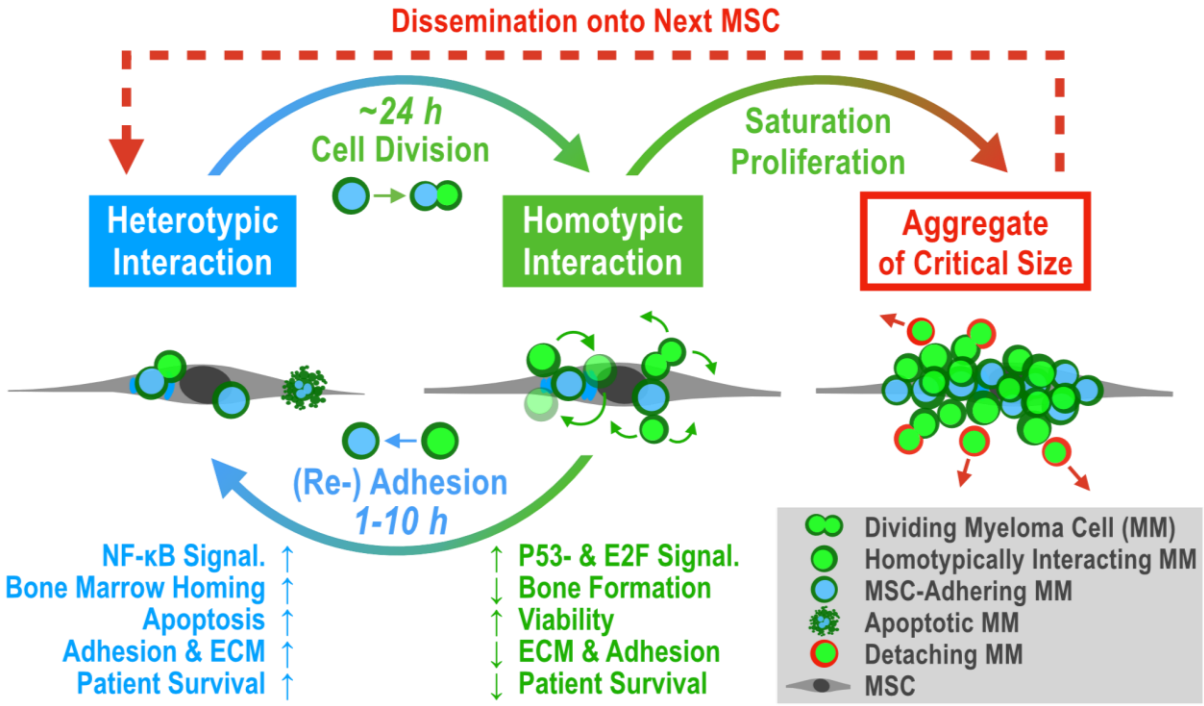

855

856

857 Tab. 1

Regulation during disease progression	Gene	Ensemble ID	Progression Free / Overall Survival	Better Prognosis with high/low expression	Association of expression with survival	
					[p-unc]	[p-adj]
Not Downregulated (or overall low expression)	**CCNE2**	**ENSG00000175305**	Overall	low	5.34E-04	8.64E-03
	MMP2	**ENSG00000087245**	Prog. Free	high	2.29E-05	2.32E-03
	OSMR	**ENSG00000145623**	Prog. Free	high	5.67E-04	7.15E-03
Continuously Downregulated (BMPC > MGUS > sMM > MM > MMR)	**AXL**	**ENSG00000167601**	Overall	high	3.64E-05	1.84E-03
	COL1A1	**ENSG00000108821**	Prog. Free	high	3.03E-04	4.37E-03
			Overall	high	5.93E-04	8.64E-03
	CXCL12	**ENSG00000107562**	Prog. Free	high	1.16E-04	2.93E-03
			Overall	high	6.48E-04	8.64E-03
	CYP1B1	**ENSG00000138061**	Overall	high	6.84E-04	8.64E-03
	DCN	**ENSG00000011465**	Overall	high	2.47E-04	8.33E-03
	LRP1	**ENSG00000123384**	Overall	high	4.34E-04	8.64E-03
	LTBP2	**ENSG00000119681**	Prog. Free	high	9.03E-05	2.93E-03
	MFAP5	**ENSG00000197614**	Prog. Free	high	2.43E-04	4.09E-03
	MMP14	**ENSG00000157227**	Prog. Free	high	6.93E-05	2.93E-03
	MYL9	**ENSG00000101335**	Prog. Free	high	1.46E-04	2.95E-03
			Overall	high	1.56E-05	1.57E-03

858

Parsed Citations

1. Blade J, Beksac M, Caers J, Jurczyszyn A, von Lilienfeld-Toal M, Moreau P, et al. Extramedullary disease in multiple myeloma: a systematic literature review. Blood Cancer Journal. 2022;12(3):1-10.
Pubmed: Author and Title
Google Scholar: Google Scholar Search

2. Rajkumar SV, Dimopoulos MA, Palumbo A, Blade J, Merlini G, Mateos M-V, et al. International Myeloma Working Group updated criteria for the diagnosis of multiple myeloma. The Lancet Oncology. 2014;15(12):e538-48.
Pubmed: Author and Title
Google Scholar: Google Scholar Search

3. Zeissig MN, Zannettino ACW, Vandyke K. Tumour Dissemination in Multiple Myeloma Disease Progression and Relapse: A Potential Therapeutic Target in High-Risk Myeloma. Cancers (Basel). 2020;12(12).

4. Akhmetzyanova I, McCarron MJ, Parekh S, Chesi M, Bergsagel PL, Fooksman DR. Dynamic CD138 surface expression regulates switch between myeloma growth and dissemination. Leukemia. 2020;34(1):245-56.
Pubmed: Author and Title
Google Scholar: Google Scholar Search

5. Garcia-Ortiz A, Rodriguez-Garcia Y, Encinas J, Maroto-Martin E, Castellano E, Teixido J, et al. The Role of Tumor Microenvironment in Multiple Myeloma Development and Progression. Cancers (Basel). 2021;13(2).

6. Aggarwal R, Ghobrial IM, Roodman GD. Chemokines in multiple myeloma. Experimental hematology. 2006;34(10):1289-95.
Pubmed: Author and Title
Google Scholar: Google Scholar Search

7. Alsayed Y, Ngo H, Runnels J, Leleu X, Singha UK, Pitsillides CM, et al. Mechanisms of regulation of CXCR4/SDF-1 (CXCL12)-dependent migration and homing in multiple myeloma. Blood. 2007;109(7):2708-17.
Pubmed: Author and Title
Google Scholar: Google Scholar Search

8. Hu X, Villodre ES, Larson R, Rahal OM, Wang X, Gong Y, et al. Decorin-mediated suppression of tumorigenesis, invasion, and metastasis in inflammatory breast cancer. Communications Biology. 2021;4(1):72.
Pubmed: Author and Title
Google Scholar: Google Scholar Search

9. Huang S-Y, Lin H-H, Yao M, Tang J-L, Wu S-J, Hou H-A, et al. Higher Decorin Levels in Bone Marrow Plasma Are Associated with Superior Treatment Response to Novel Agent- Based Induction in Patients with Newly Diagnosed Myeloma - A Retrospective Study. PloS One. 2015;10(9):e0137552.
Pubmed: Author and Title
Google Scholar: Google Scholar Search

10. Katz B-Z. Adhesion molecules-The lifelines of multiple myeloma cells. Seminars in Cancer Biology. 2010;20(3):186-95.
Pubmed: Author and Title
Google Scholar: Google Scholar Search

11. Kibler C, Schermutzki F, Waller HD, Timpl R, Muller CA, Klein G. Adhesive interactions of human multiple myeloma cell lines with different extracellular matrix molecules. Cell Adhesion and Communication. 1998;5(4):307-23.
Pubmed: Author and Title
Google Scholar: Google Scholar Search

12. Glavey SV, Naba A, Manier S, Clauser K, Tahri S, Park J, et al. Proteomic characterization of human multiple myeloma bone marrow extracellular matrix. Leukemia. 2017;31(11):2426-34.
Pubmed: Author and Title
Google Scholar: Google Scholar Search

13. Sanz-Rodriguez F, Ruiz-Velasco N, Pascual-Salcedo D, Teixido J. Characterization of VLA-4-dependent myeloma cell adhesion to fibronectin and VCAM-1: VLA-4-dependent Myeloma Cell Adhesion. British Journal of Haematology. 1999;107(4):825-34.
Pubmed: Author and Title
Google Scholar: Google Scholar Search

14. Chatterjee M, Honemann D, Lentzsch S, Bommert K, Sers C, Herrmann P, et al. In the presence of bone marrow stromal cells human multiple myeloma cells become independent of the IL-6/gp130/STAT3 pathway. Blood. 2002;100(9):3311-8.
Pubmed: Author and Title
Google Scholar: Google Scholar Search

15. Hideshima T, Mitsiades C, Tonon G, Richardson PG, Anderson KC. Understanding multiple myeloma pathogenesis in the bone marrow to identify new therapeutic targets. Nature Reviews Cancer. 2007;7(8):585-98.
Pubmed: Author and Title
Google Scholar: Google Scholar Search

16. Frassanito MA, Cusmai A, Iodice G, Dammacco F. Autocrine interleukin-6 production and highly malignant multiple myeloma: relation with resistance to drug-induced apoptosis. Blood. 2001;97(2):483-9.
Pubmed: Author and Title
Google Scholar: Google Scholar Search

17. Urashima M, Chauhan D, Uchiyama H, Freeman G, Anderson K. CD40 ligand triggered interleukin-6 secretion in multiple myeloma. Blood. 1995;85(7):1903-12.
Pubmed: Author and Title
Google Scholar: Google Scholar Search

18. Solimando AG, Malerba E, Leone P, Prete M, Terragna C, Cavo M, et al. Drug resistance in multiple myeloma: Soldiers and weapons in the bone marrow niche. Frontiers in Oncology. 2022;12:973836.
Pubmed: Author and Title
Google Scholar: Google Scholar Search

19. Ghobrial IM. Myeloma as a model for the process of metastasis: implications for therapy. Blood. 2012;120(1):20-30.
Pubmed: Author and Title
Google Scholar: Google Scholar Search

20. Dziadowicz SA, Wang L, Akhter H, Aesoph D, Sharma T, Adjeroh DA, et al. Bone Marrow Stroma-Induced Transcriptome and Regulome Signatures of Multiple Myeloma. Cancers. 2022;14(4):927.
Pubmed: Author and Title
Google Scholar: Google Scholar Search

21. Seckinger A, Delgado JA, Moser S, Moreno L, Neuber B, Grab A, et al. Target Expression, Generation, Preclinical Activity, and Pharmacokinetics of the BCMA-T Cell Bispecific Antibody EM801 for Multiple Myeloma Treatment. Cancer Cell. 2017;31(3):396- 410.
Pubmed: Author and Title
Google Scholar: Google Scholar Search

22. Seckinger A, Hillengass J, Emde M, Beck S, Kimmich C, Dittrich T, et al. CD38 as Immunotherapeutic Target in Light Chain Amyloidosis and Multiple Myeloma-Association With Molecular Entities, Risk, Survival, and Mechanisms of Upfront Resistance. Frontiers in Immunology. 2018;9:1676.
Pubmed: Author and Title
Google Scholar: Google Scholar Search

23. Burger R, Guenther A, Bakker F, Schmalzing M, Bernand S, Baum W, et al. Gp130 and ras mediated signaling in human plasma cell line INA-6: a cytokine-regulated tumor model for plasmacytoma. The Hematology Journal: The Official Journal of the European Haematology Association. 2001;2(1):42-53.
Pubmed: Author and Title
Google Scholar: Google Scholar Search

24. Gramatzki M, Burger R, Trautman U, Marschalek R, Lorenz H, Hansen-Hagge TE, et al. Two new interleukin-6 dependent plasma cell lines carrying a chromosomal abnormality involving the IL-6 gene locus. 1994;84 Suppl. 1:173a-a.
Pubmed: Author and Title
Google Scholar: Google Scholar Search

25. Anders S, Pyl PT, Huber W. HTSeq--a Python framework to work with high- throughput sequencing data. Bioinformatics (Oxford, England). 2015;31(2):166-9.
Pubmed: Author and Title
Google Scholar: Google Scholar Search

26. Dobin A, Davis CA, Schlesinger F, Drenkow J, Zaleski C, Jha S, et al. STAR: ultrafast universal RNA-seq aligner. Bioinformatics. 2013;29(1):15-21.
Pubmed: Author and Title
Google Scholar: Google Scholar Search

27. Zerbino DR, Achuthan P, Akanni W, Amode M R, Barrell D, Bhai J, et al. Ensembl 2018. Nucleic Acids Research. 2018;46(D1):D754-D61.
Pubmed: Author and Title
Google Scholar: Google Scholar Search

28. Zhou Y, Zhou B, Pache L, Chang M, Khodabakhshi AH, Tanaseichuk O, et al. Metascape provides a biologist-oriented resource for the analysis of systems-level datasets. Nature Communications. 2019;10(1):1523.
Pubmed: Author and Title
Google Scholar: Google Scholar Search

29. Seabold S, Perktold J, editors. Statsmodels: Econometric and statistical modeling with python. Proceedings of the 9th Python in Science Conference; 2010: Austin, TX.

30. Vallat R. Pingouin: statistics in Python. Journal of Open Source Software. 2018;3(31):1026.
Pubmed: Author and Title
Google Scholar: Google Scholar Search

31. Kuric M, Ebert R. plotastic: Bridging Plotting and Statistics in Python. The Journal of Open Source Software. 2024.
Pubmed: Author and Title
Google Scholar: Google Scholar Search

32. Hothorn T, Lausen B. Maximally Selected Rank Statistics in R. R News. 2002;2:3-5.
Pubmed: Author and Title
Google Scholar: Google Scholar Search

33. Kuric M, Ebert R. markur4/Supplemental-INA-6-Subpopulations-and-Aggregation- Detachment-Dynamics: Supplementary Data [

34. Kawano MM, Huang N, Tanaka H, Ishikawa H, Sakai A, Tanabe O, et al. Homotypic cell aggregations of human myeloma cells with ICAM-1 and LFA-1 molecules. British Journal of Haematology. 1991;79(4):583-8.
Pubmed: Author and Title
Google Scholar: Google Scholar Search

35. Okuno Y, Takahashi T, Suzuki A, Ichiba S, Nakamura K, Okada T, et al. In vitro growth pattern of myeloma cells in liquid suspension or semi-solid culture containing interleukin-6. International Journal of Hematology. 1991;54(1):41-7.

Pubmed: Author and Title
Google Scholar: Google Scholar Search

36. Blonska M, Zhu Y, Chuang HH, You MJ, Kunkalla K, Vega F, et al. Jun-regulated genes promote interaction of diffuse large B-cell lymphoma with the microenvironment. Blood. 2015;125(6):981-91.
Pubmed: Author and Title
Google Scholar: Google Scholar Search

37. Tai Y-T, Li X-F, Breitkreutz I, Song W, Neri P, Catley L, et al. Role of B-cell-activating factor in adhesion and growth of human multiple myeloma cells in the bone marrow microenvironment. Cancer Research. 2006;66(13):6675-82.
Pubmed: Author and Title
Google Scholar: Google Scholar Search

38. Standal T, Seidel C, Plesner T, Sanderson R, Waage A, Borset M, et al. Osteoprotegerin is bound, internalized, and degraded by multiple myeloma cells. Blood. 2002;100:3002-7.
Pubmed: Author and Title
Google Scholar: Google Scholar Search

39. Van Valckenborgh E, Croucher PI, De Raeve H, Carron C, De Leenheer E, Blacher S, et al. Multifunctional role of matrix metalloproteinases in multiple myeloma: a study in the

5. T2MM mouse model. Am J Pathol. 2004;165(3):869-78.
Pubmed: Author and Title
Google Scholar: Google Scholar Search

40. Zhou F, Meng S, Song H, Claret FX. Dickkopf-1 is a key regulator of myeloma bone disease: opportunities and challenges for therapeutic intervention. Blood reviews. 2013;27(6):261-7.
Pubmed: Author and Title
Google Scholar: Google Scholar Search

41. Sprynski AC, Hose D, Caillot L, Reme T, Shaughnessy JD, Barlogie B, et al. The role of IGF-1 as a major growth factor for myeloma cell lines and the prognostic relevance of the expression of its receptor. Blood. 2009;113(19):4614-26.
Pubmed: Author and Title
Google Scholar: Google Scholar Search

42. Tabolacci C, De Martino A, Mischiati C, Feriotto G, Beninati S. The Role of Tissue Transglutaminase in Cancer Cell Initiation, Survival and Progression. Medical Sciences. 2019;7(2):19.
Pubmed: Author and Title
Google Scholar: Google Scholar Search

43. Bao L, Lai Y, Liu Y, Qin Y, Zhao X, Lu X, et al. CXCR4 is a good survival prognostic indicator in multiple myeloma patients. Leukemia Research. 2013;37(9):1083-8.
Pubmed: Author and Title
Google Scholar: Google Scholar Search

44. Sarin V, Yu K, Ferguson ID, Gugliemini O, Nix MA, Hann B, et al. Evaluating the efficacy of multiple myeloma cell lines as models for patient tumors via transcriptomic correlation analysis. Leukemia. 2020;34(10):2754-65.
Pubmed: Author and Title
Google Scholar: Google Scholar Search

45. Dotterweich J, Schlegelmilch K, Keller A, Geyer B, Schneider D, Zeck S, et al. Contact of myeloma cells induces a characteristic transcriptome signature in skeletal precursor cells -Implications for myeloma bone disease. Bone. 2016;93:155-66.
Pubmed: Author and Title
Google Scholar: Google Scholar Search

46. Wadgaonkar R, Phelps KM, Haque Z, Williams AJ, Silverman ES, Collins T. CREB- binding protein is a nuclear integrator of nuclear factor-kappaB and p53 signaling. The Journal of Biological Chemistry. 1999;274(4):1879-82.

Pubmed: Author and Title
Google Scholar: Google Scholar Search

47. Webster GA, Perkins ND. Transcriptional Cross Talk between NF-kB and p53. Molecular and Cellular Biology. 1999;19(5):3485-95.
Pubmed: Author and Title
Google Scholar: Google Scholar Search

48. Polager S, Ginsberg D. p53 and E2f: partners in life and death. Nature Reviews Cancer. 2009;9(10):738-48.
Pubmed: Author and Title
Google Scholar: Google Scholar Search

49. Hose D, Reme T, Hielscher T, Moreaux J, Messner T, Seckinger A, et al. Proliferation is a central independent prognostic factor and target for personalized and risk-adapted treatment in multiple myeloma. Haematologica. 2011;96(1):87-95.
Pubmed: Author and Title
Google Scholar: Google Scholar Search

50. Garces J-J, Simicek M, Vicari M, Brozova L, Burgos L, Bezdekova R, et al. Transcriptional profiling of circulating tumor cells in multiple myeloma: a new model to understand disease dissemination. Leukemia. 2020;34(2):589-603.
Pubmed: Author and Title
Google Scholar: Google Scholar Search

51. Brandl A, Solimando AG, Mokhtari Z, Tabares P, Medler J, Manz H, et al. Junctional adhesion molecule C expression specifies a CD138low/neg multiple myeloma cell population in mice and humans. Blood Advances. 2022;6(7):2195-206.
Pubmed: Author and Title
Google Scholar: Google Scholar Search

52. Wong AD, Searson PC. Mitosis-mediated intravasation in a tissue-engineered tumor- microvessel platform. Cancer research. 2017;77(22):6453-61.
Pubmed: Author and Title
Google Scholar: Google Scholar Search

53. Maichl DS, Kirner JA, Beck S, Cheng W-H, Krug M, Kuric M, et al. Identification of NOTCH-driven matrisome-associated genes as prognostic indicators of multiple myeloma patient survival. Blood Cancer Journal. 2023;13(1):1-6.
Pubmed: Author and Title
Google Scholar: Google Scholar Search

54. Bou Zerdan M, Nasr L, Kassab J, Saba L, Ghossein M, Yaghi M, et al. Adhesion molecules in multiple myeloma oncogenesis and targeted therapy. International Journal of Hematologic Oncology. 2022;11(2):IJH39.
Pubmed: Author and Title
Google Scholar: Google Scholar Search

55. Evers M, Schreder M, Stuhmer T, Jundt F, Ebert R, Hartmann TN, et al. Prognostic value of extracellular matrix gene mutations and expression in multiple myeloma. Blood Cancer Journal. 2023;13(1):43.
Pubmed: Author and Title
Google Scholar: Google Scholar Search